AIAA AVIATION Forum
August 2-6, 2021, VIRTUAL EVENT
AIAA AVIATION 2021 FORUM

10.2514/6.2021-2418

Preliminary Design of a Trans-Atlantic High Speed Civil Transport

Luke Frost,[1] Vern Chia, [1] Josh Reuland, [1] Shinji Namera, [1] Ethan Moreno[1]

and

Timothy T. Takahashi[2]

Arizona State University, Tempe, Arizona, 85281

This design study proposes supersonic, 128 seat passenger aircraft sized for the North Atlantic market. The team developed, integrated and used a collection of legacy and newly authored tools to perform trade studies. These studies led to an optimized design that maximized specific range at a maximum required still air distance. The proposed design uses four current technology turbofan engines without afterburner equipped with normal shock inlets. While the proposed aircraft is slower than Concorde, it significantly lowers the fuel burn per seat mile compared to its supersonic passenger predecessors while offering a comfortable interior for daylight flights. The team engineered the aircraft to be compliant with current 14 CFR § 25 regulations and meets takeoff, landing, and runway requirements at commercial airports used to service Trans-Atlantic flights.

[1] Undergraduate Student, Aerospace Engineering, Arizona State University, AIAA Student Member.
[2] Professor of Practice, Aerospace Engineering, Arizona State University, Associate Fellow AIAA.

I. Introduction

THE history of commercial aircraft is a long one, with dozens of iconic subsonic aircraft developed, however, the history of supersonic commercial aircraft is a difficult one. Because of the characteristics of supersonic flight, with the development of shocks along a wing, supersonic aircraft have to be designed differently than their subsonic counterparts. Due to how devastating a shock can be on performance, supersonic aircraft have swept and thin wings. While this design benefits supersonic flight performance it has negative effects on subsonic flight, as the swept and thinner wings have worse performance at subsonic flight speeds. It is impossible to have a perfect aircraft that performs best in both regimes, as every change will affect some other aspect of the aircraft. It is for these reasons that a choice has to be made as to what the aircraft should be built for. Only two commercial aircraft, the Concorde [1] and the Tupolev Tu-144 [1] have entered service; the Tu-144 having an extremely limited operational life. While the Concorde and Tupolev planned to change aviation forever, they were not destined to do so.

The Concorde was developed by the British Aircraft Corporation and Aérospatiale, and was a joint effort between Great Britain and France. [1] The goal was to develop the first subsonic passenger commercial aircraft, to serve for Trans-Atlantic flight routes. [1] The first flight was made on September 26, 1976 and entered service in May of that year. [1] The Concorde itself had a maximum takeoff weight of 408,000 pounds, could carry 128 passengers, had a maximum Mach number of 2.04, a maximum cruise altitude of 60,000 feet, and a range of 3,914 -NM [1]. It was for these reasons, as well as the "high class" nature of the experience that made the Concorde a beacon of what was possible in aviation, not only in terms of technology but also in terms of experience. The journey of the Concorde was not perfect, as on July 25, 2000 a flight from Paris to New York City burst into flames due to debris causing an engine failure on takeoff, resulting in the deaths of all 109 people on board. [1] Three years later on October 24, 2003 the Concorde was retired due to the high costs of operation. [1]

FIGURE 1 – BaE CONCORDE

The only other supersonic transport aircraft was the Russian Tu-144. While not as well known as the Concorde, the Tu-144 was developed to be in direct competition with the Concorde, as the Soviets wanted to develop their own supersonic transport. [2] The Tu-144 had a maximum takeoff weight of 397,000 pounds, a maximum Mach number of 2.35, a range of 3,510 -NM, had a capacity of 140 passengers, and a maximum altitude of 59,700 feet. [2] The similarities between the Tu-144 and Concorde are not easy to miss, not only in terms of performance, but in appearance as well. The overall stability of the Tu-144 was put into question as it had two crashes, one at a Paris air show in 1973, and in Yegoryevsk, in 1978. [2] In the same year, the Tu-144 was retired from passenger service, and would be retired entirely in 1999. [2]

FIGURE 2 – Tupolev Tu-144

No supersonic airliners currently fly. Their retirement was due to their cost of operation, along with other factors. The cost of operation was the key determinant in the decision to retire the Concorde especially. [3] In the end it was the Concorde that would become the most famous of the two, and synonymous with supersonic commercial travel.

We propose and substantiate a Mach 1.5 cruise supersonic transport aircraft with a 128 business class seat interior. This aircraft is capable of flying from the east coast of the United States to European countries across the North Atlantic. Due to developments in airbreathing propulsion systems, this aircraft uses quieter more efficient engines

than the Concorde, allowing it to be more economically efficient than the Concorde ever could be. While supersonic aircrafts have been left on the sidelines in the last two decades, with the ***Atlantic Shuttle*** supersonic travel is not only possible once again but more lucrative and viable than ever.

II. Defining the Mission Requirements

The launching point for this project was to define the market segment and derive the mission requirements for the aircraft. Here, we survey the entire Trans-Atlantic premium market from 2019 and determine the most stressing sizing mission.

The major carriers across the North Atlantic include British Airways [4] and Virgin Atlantic Airways [4] from the UK, AirFrance/KLM [4], based out of France and the Netherlands respectively, Lufthansa [4] from Germany, Air Canada from Canada, and the U.S. based big-three airlines United Airlines, American Airlines and Delta Airlines.

With our customers found, we are able to start to determine possible flight paths that would be beneficial to each company involved.

Table 1: Destination and Runways

Airport	CODE	Primary Runway TORA	Primary Runway LDA	Elevation	Carriers
New York / JFK	JFK	14,511-ft and 12,079-ft	12,468-ft and 7,795 ft	~12-ft	AF, AA (HUB), BA, DL (HUB), LH, VA
Newark	EWR	11,000-ft and 10,000 ft	8460-ft and 8810 ft	~10-ft	UA (HUB), BA, LH
Philadelphia	PHL	12,000-ft	12,000ft	~20-ft	AA (HUB), BA, LH
Washington/Dulles	IAD	11,500-ft and 11,500-ft	11,500-ft and 11,500-ft	~300-ft	AA, KL, LH, UA (HUB), VA
Atlanta/Hartsfield	ATL	12,390-ft	11,730-ft	~1019-ft	AF, BA, DL (HUB), KL, VA
Toronto/Pearson	YYZ	11,120-ft	10,985-ft	~569-ft	AC (HUB), KL, LH
Montreal/Trudeau	YUL	11,000-ft	11,000-ft	~96-ft	AC (HUB),AF, BA, KLM, LH
London/Heathrow	LHR (EGLL)	12,798-ft	12,736-ft	~82-ft	AA, AC, BA (HUB), DL, UA, VA (HUB)
Amsterdam/Schiphol	AMS (EHAM)	12,467-ft and 11,482-	12,467-ft and 11,482-ft	Sea-level	AA, AC, DL, KLM (HUB), UA
Paris/De Gaulle	CDG (LPHG)	13,589-ft and 12,709-ft	13,589-ft and 11,811-ft	~331-ft	AA, AC, AF (HUB), DL, UA
Frankfurt am Main	FRA (EDDF)	13,123-ft	13,123-ft	~360-ft	AA, AC, DL, LH (HUB),UA

In Table 1, we see a listing of all of the probable airports that comprise the major North Atlantic premium traveler market. The North American airports include JFK and Newark in the New York City area, Philadelphia, Washington, Atlanta, Toronto and Montreal. The European airports include London/Heathrow, Amsterdam/Schiphol, Paris/De Gaulle and Frankfurt. A common pattern emerges; these major gateway airports often serve as a hub for one of the principal first-world airlines. These airports are all near sea-level; they all feature long primary runways.

Being a supersonic commercial airliner for Trans-Atlantic flight, there are restrictions as to when supersonic flight can occur. The sonic boom that is generated when the aircraft goes supersonic, is not only very disruptive to anyone in the vicinity, but can potentially cause damage to nearby structures. Because of this, there are regulations that prohibit supersonic flight over mainland United States and Europe. This resulted in the flight path having to be adjusted. This

was done by taking the shortest path to the Atlantic Ocean upon takeoff. This would get the aircraft off of land, and therefore safe to proceed to supersonic flight.

The team decided that the most stressing missions would be operated by Delta Airlines and KLM Airlines. The four defining sizing missions would be Atlanta to Amsterdam and return, Atlanta to Paris/CDG and return; see FIGURE 3 (overleaf). The high volume New York market would need to be operated with a minimal over-land route, thus a southerly routing from JFK or EWR to AMS and CDG define the economic mission; also see FIGURE 3 (overleaf).

The final component of our mission requirements was to determine if a supersonic airliner was economically viable. This was done by observing flights from our arrival and destinations to see how many seats in business and first class were used. We specifically looked at these seats because of how expensive a supersonic flight would cost. From this we found that on average nearly 98% of the seats offered on our flights were booked. This indicated that there was a market for the aircraft. By looking at how many average passengers were on these flights per day, we concluded that a flight of 128 business class interior seats would be sufficient in order to be cost effective.

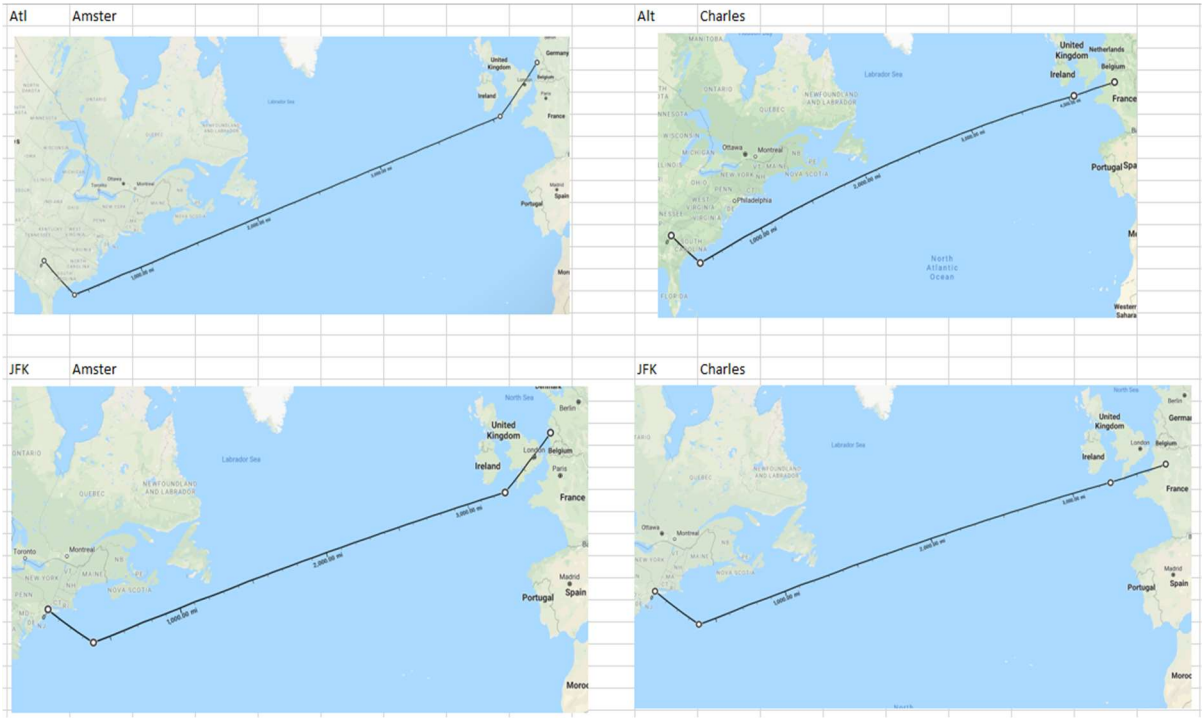

FIGURE 3: Flight Paths for critical sizing / marketing missions

Our design speed needs to be fast enough to allow for convenient connecting flights allowing for the time change between Europe and the United States. The mission should begin in the early morning at a European gateway airport and fly to North America, ensuring that the plane would arrive at a reasonable time for passengers to catch a connecting flight. Similarly, the North American departure should be late morning (allowing for a domestic US connection) while arriving into Europe before airport curfews, so that passengers could clear customs and check into a nearby hotel.

According to our research, both Charles de Gaulle and Schiphol Airport have restrictive measures for nighttime runway use. For Schiphol, night operations are restricted to a single take-off runway and a single landing runway between 23:00 and 06:00[5]. Charles de Gaulle has a limit on the number of take-offs and landings between 00:30 and 05:29 in order to reduce noise pollution [6].

An accurate estimation of arrival and departure times can be made by calculating flight time using KTAS and ESAD. The ground track distance used for our ESAD numbers was calculated using Google Maps, by drawing out the

intended flight paths between city pairs and measuring that distance (shown in FIGURE 3). Table 2 shows that the departure and arrival times fall outside of the allocated curfew.

Table 2: Example Flight Times

City Pairs	Dep Time	Arr Time (incl. 1 hr ground time)	Ground Dist	ESAD w/ Winds	Flight Time @ 690 KTAS
JFK to CDG	8:30am EDT	8:03pm CEST	3756-NM	3491-NM	5 Hrs : 3Mins
JFK to AMS	10:26am EDT	10:00pm CEST	3393-NM	3154-NM	4 Hrs : 34 Mins
ATL to AMS	7:30am EDT	7:56 pm CEST	4028-NM	3745-NM	5 Hrs :26 Mins
ATL to CDG	9:40am EDT	10:00pm CEST	3966-NM	3687-NM	5 Hrs : 20 Mins
AMS to ATL	8:20pm CEST	10:00pm EDT	4028-NM	4596-NM	6 Hrs : 40 Mins
CDG to ATL	7:30am CEST	9:04 am EDT	3966-NM	4525-NM	6 Hrs : 34Mins
CDG to JFK	8:48pm CEST	10:00pm EDT	3756-NM	4286-NM	6 Hrs : 12 Mins
AMS to JFK	8:30am CEST	9:07 am EDT	3393-NM	3872-NM	5 Hrs : 37Mins

To better explain how we computed our ESAD, the team decided to use real data to estimate the true wind patterns along our flight path. By visiting the University of Wyoming's Department of Atmospheric Science, we were able to find the actual weather patterns along a flight path similar to our own. Taking data points from Atlanta, Bermuda, Camborne, and Norderney using a year of data we were able to find out the true seasonal averages of wind speed, as well as maximum wind speeds. This allowed us to conclude that the maximum wind speed was 85.3 knots headwind for flights from Europe to North America and 50 knot tailwinds in the opposite direction.

CHARLESTON			BERMUDA			CAMBORNE			NORDERNEY		
HGHT	DRCT	SKNT	HGHT	DRCT	SKNT	HGHT	DRCT	SKNT	HGHT	DRCT	SKNT
m	deg	knot	m	deg	knot	m	deg	knot	m	deg	knot
15	190	4	37	260	12	88	190	10	11	190	10
117	203	14	178	255	18	364	205	26	78	210	23
168	210	19	305	260	20	476	209	27	136	215	25
176	210	19	610	265	20	640	215	28	203	220	27
211	210	19	840	260	20	719	215	28	364	240	27
305	210	19	914	265	20	817	215	28	407	241	27
392	210	18	1219	275	19	871	215	28	720	245	29
515	210	17	1266	278	19	925	215	28	1105	242	30
610	210	16	1533	294	22	1162	222	27	1401	240	31
720	210	20	1543	295	22	1227	224	27	1572	245	31
820	210	23	1700	298	22	1245	224	27	1764	250	31
829	210	23	1829	300	22	1264	225	27	1862	248	32
866	210	23	1840	300	22	1283	226	28	2243	241	36
914	210	23	2134	300	24	1311	227	29	2264	241	36
1219	230	13	2438	310	27	1367	229	31	2305	240	37
1442	234	13	2743	305	27	1405	230	32	2326	240	37
1524	235	13	3048	310	32	1500	234	33	2388	240	36
1540	245	9	3130	305	32	1529	235	33	2771	240	33
1769	249	10	3188	303	32	1539	235	33	2925	240	31
1829	250	10	3658	290	33	1548	235	33	3583	230	33
1972	264	9	4267	295	39	1743	230	31	4086	234	30
2134	280	8	4357	296	40	1832	234	31	4247	235	29
2295	288	12	4436	298	41	1952	240	30	5440	250	33
2438	295	15	4543	300	43	1972	239	30	7010	265	35

FIGURE 4: University of Wyoming atmosphere data

Seasonal Wind Speeds Along Flight Path				
	CHARLESTON	BERMUDA	CAMBORNE	NORDERNEY
SPRING				
MARCH	76.45454545	85.3	18.26666667	22.09090909
APRIL	62.57142857	21.76923077	21.76923077	27
MAY	35.71428571	14.66666667	14.66666667	13.125
max (KNOT)	76.45454545	85.3	21.76923077	27
SUMMER				
June	16.51724138	31	22.8	14.81818182
July	14.66666667	36.25	36.25	18.8
August	16.60869565	20.71428571	20.71428571	28.11764706
max (KNOT)	16.60869565	36.25	36.25	28.11764706
FALL				
September	20.44	10.58333333	31.83333333	25.15384615
October	39.11764706	23.35714286	23.35714286	20.69230769
November	60.84615385	33.375	33.375	23.5
max (KNOT)	60.84615385	33.375	33.375	25.15384615
WINTER				
December	59.23529412	72.125	26.6666667	33.0666667
January	56.875	43.77778	43.7777778	58.1818182
February	78.22222222	35.25	35.25	23.3333333
max (KNOT)	78.22222222	72.125	43.7777778	58.1818182

FIGURE 5: Wind Speeds Along Flight Path Calculations

Miles					
From	Sub	Super	Sub	To	
Atl	365	3705	568	Amster	
Atl	375	3685	507	Charles	
JFK	380	2910	553	Amster	
JFK	380	2910	466	Charles	
nm					
From	Sub	Super	Sub	To	
Atl	316.973684	3217.5	493.263157	Amster	4027.73684
Atl	325.657894	3200.13157	440.289473	Charles	3966.07894
JFK	330	2527.10526	480.236842	Amster	3337.34210
JFK	330	2527.10526	404.684210	Charles	3261.78947

FIGURE 6: Example ESAD Calculation

Between TABLE 2 and FIGURE 6, we see still-air-distances for our various flight plans. As it can be seen, the longest flight, in terms of Nautical Miles flown will be from Atlanta to Amsterdam with nearly 4028 -NM flown on that flight path. It is also important to note that the distances of subsonic and supersonic portions of the flight have been calculated, and the flight will average about 80% supersonic flight time, and 20% subsonic.

sub 1 esad	sub 2 esad
379.2405144	590.1491721
Subsonic miles	Supersonic miles
969.3896865	3670.862631
total ESAD	4640.252317

East to West

sub 1 esad	sub 2 esad
289.0562516	449.8190436
Subsonic miles	Supersonic miles
738.8752952	2999.583731
total ESAD	3738.459026

West to East

FIGURE 7: Longest ESAD for East to West and West to East Flights

Using all the data collected the flight ESAD could be found for the longest east to west flight, as well as the longest west to east flight, with a total of ~4640-NM and ~3738-NM respectively. This makes sense, as flying from the United States to Europe has a tailwind, which essentially is pushing the aircraft forward, allowing for a shorter ESAD than a European to North America flight, where you are flying into the wind. With the ESAD found for a tailwind and headwind, we made further optimizations to the mission, by creating a flight plan unique to the aircraft.

III. Certification Requirements - Code of Federal Regulations

In order for the aircraft to be certified to fly it has to be in compliance with Federal Aviation Administrations (FAA), which is done by following the Code of Federal Regulations (CFR), specifically under Title 14 regulations, [7] [8] [9] as well as following European Union Regulations (EUROPA). [10] For these reasons, the aircraft designed follows federal regulations so that it is certified to fly internationally. Below is a list, with descriptions of the key CFR's the aircraft needed to meet.

14 CFR § 25.105 - Takeoff explains the requirements of runway length and check if that distance is sufficient enough for takeoff. This regulation is correlated with 14 CFR § 25.107, 14 CFR § 25.109, 14 CFR § 25.111, 14 CFR § 25.113, and 14 CFR § 25.115.

14 CFR § 25.107 - Takeoff Speeds describes the takeoff decision speed, where the pilots determine whether they reject or continue takeoff due to engine failure. If an aircraft continues takeoff, it has to reach the takeoff safety speed, *V2*, at 35 ft above the runway.

14 CFR § 25.119 - Landing Climb: All Engines Operating explains the minimum climb capability in the landing configuration and shows that steady climb gradient must be greater than 3.2 % for 4-engine aircraft.

14 CFR § 25.121 - Climb. One-Engine-Inoperative states the minimum climb gradient capability for 1st segment climb, 2nd segment climb, and final takeoff. For 4-engine aircraft, steady climb gradient may not be less than 1.7 % for the final takeoff phase.

14 CFR § 25.125 - Landing states that *VREF* must be greater than either 1.23 times stall speed in the landing configuration and not less than *VMCL*.

14 CFR § 25.149 - Minimum Control Speed defines the minimum airspeed where aerodynamic trim can balance against an engine failure. Three speeds fall out of this regulation: minimum control speed on the ground (*VMCG*), in the air with takeoff (*VMCA*) or landing (*VMCL*) flaps deployed.

14 CFR § 25.237 - Wind Velocities describes that an aircraft must have sufficient control to demonstrate to be safe in the crosswind at least 20 knots or 0.2 times stall speed for both takeoff and landing configurations.

14 CFR § 25.303 - Factor of Safety requires to use the factor of safety of 1.5 to the limit unless it is specified to hold the safety margin of structures. If the limit load is established in terms of ultimate load, safety factor does not have to be applied.

14 CFR § 25.305 - Strength and Deformation states that the aircraft structure must be able to support any loads up to limit load without detrimental deformation and also withstand the ultimate loads for three seconds. However, if the evidence of strength of structure is shown by the simulation of dynamic tests, this limit of ultimate load does not apply. The analytical proof can also be used, as long as it can show that the deformation does not have a significant effect and deformations are fully accounted for in the analysis with sufficient assumptions.

14 CFR § 25.333 and 337 - Flight Maneuvering envelope describes that the strength requirements of the structure must be satisfied for all combinations of load factor and equivalent airspeed shown on V-n diagram. The Limit Maneuvering Load Factors for a large airplane, like this, specifies limit load factors of +2.5-gee and -1.0-gee.

14 CFR § 25.365 - Pressurized Compartment Loads states that the aircraft structure must be able to withstand the loads due to the pressure differential due to the engine disintegration. Pressure distribution and stress concentration should be taken into account.

14 CFR § 25.613 - Material Strength Properties and Material Design Values states that engineers must choose the material design values such that it can minimize the probability of structural failure and use “99 % probability and 95 % confidence” ratings, also known as A-basis materials rating in MIL HDBK-5. [11])

14 CFR § 25.807 - Emergency Exit covers the possible emergency exit doors that can be mounted on an aircraft. Type A, B, C are floor-level doors yet with different sizing: 42 inches wide by 72 inches tall for Type A, 32 inches wide by 72 inches tall for Type B, and 30 inches wide by 48 inches tall for Type C. In addition to those, there are some other emergency doors from Type I to Type IV: at least 24 inches wide by 48 inches tall floor-level door for Type I, at least 20 inches wide by 44 inches tall door for Type II in which the gap needs to be less than 10 inches for step-up inside aircraft or 17 inches step-down outside aircraft, at least 20 inches wide by 36 inches tall door for Type III in which the gap needs to be less than 20 inches for step-up inside aircraft or 27 inches step-down outside aircraft, and at least 19 inches wide by 26 inches tall door for Type IV in which the gap needs to be less than 29 inches for step-up inside aircraft or 36 inches step-down outside aircraft. Types and numbers of doors required to mount on an aircraft depend on the number of passengers.

14 CFR § 25.815 - Aisle covers the width of the aisle necessary between seats for an aircraft depending on the number of passengers. For the aircraft with 20 or more passengers, the aisle width must be 20 inches or more.

14 CFR § 25.841 - Pressurized Cabin describes the restriction of pressure altitude. It requires an aircraft to be equipped so that the pressure altitude should not exceed 8,000 ft under normal operation. For exceptions, if certification of aircraft above 25,000 ft is requested, then passengers in the aircraft should not be exposed to the pressure altitude of 15,000 ft after pressurization system failure. Also, the aircraft must be designed in a way that the pressure altitude after decompression must not be in excess of 25,000 ft for more than 2 minutes, or 40,000 ft for any duration.

14 CFR § 91.167 - Fuel Requirements for Flight in IFR Conditions governs an aircraft under IFR conditions and restrict the aircraft operation unless it carries enough fuel to fly to the first point of intended landing, to fly from that airport to the alternate airport, or to fly for 45 minutes after that at normal cruising speed.

14 CFR § 91.533 - Flight Attendant Requirements states how many flight attendants need to be on board given the amount of passengers. With a passenger capacity of 128 and scheduled flight times less than 8 hours, there will be a total of three flight attendants on board.

14 CFR § 91.817 - Civil Aircraft Sonic Boom: states that no person can operate a civil aircraft in the United States with a Mach number greater than 1.0.

14 CFR § 91.821 - Civil Supersonic Airplane Noise Limits cites that except for the Concorde that has flight times after January 1, 1980, no person can operate a supersonic civil aircraft that is not in compliance with Stage 2 noise limits, which went into effect on October 13, 1977.

14 CFR § 121.189 - Airplanes: Turbine Engine Powered: Takeoff Limitations states that it restricts the flight of an aircraft with a weight greater than it is shown in the Airplane Flight Manual. Pilots must comply with those situations before attempting to takeoff.

14 CFR § 121.195 - Airplanes: Turbine Engine Powered: Landing Limitations states that it restricts the flight of an aircraft, if the weight on arrival may exceed the landing weight that is set on the Airplane Flight Manual. Under this limitation, pilots are required to multiply the actual landing distance by 1.67 factor to compute the runway length.

IV. Design Analysis and Synthesis Tools

A. Weight Estimation

Weight estimation is a complex and tedious task. The complexity arises from the fact that everything influences everything when it comes to weight. Our weight estimation tool was built using Professor Takahashi's supplied weight spreadsheet, which utilizes equations derived from Professor Torenbeek's *Synthesis of Aircraft Design*, [12] Niu's *Airframe Structural Design* [13] as well as Professor Takahashi's *Aircraft Performance and Sizing Volumes I & II.* [14][15] The inputs for this tool include variables such as wingspan, max Mach number, and fuselage length among others. The outputs obtained from this include payload, *MZFW*, *OEW*, *MLW* and *MTOW*. These weights are essential to the sizing and synthesis of our aircraft. They affect various performance parameters, and ultimately affect the mission the aircraft is designed to do. In order to ensure the weight estimation tool functioned correctly, actual published values for the 737 and 747 (from marketing literature) [16] [17] were used to validate the results.

OUTPUTS					
W/Sref	109.3	lb/ft^2			
T/W	0.261				
CHT	0.247				
CVT	0.031				
STRUCTURAL WEIGHT		150860.4	lbm		
W_wing_primary_structure	83690		lbm		
W_horizontal_tail	2345		lbm		
W_vertical_tail	972		lbm		
W_fins	0		lbm		
W_fuselage	29106		lbm		
W_nosewheel	2112		lbm		
W_mainwheel	13942		lbm		
W_aerocontrol surfaces	4979		lbm		
"crud weight"	13715		lbm		
PROPULSION WEIGHT		26446.0	lbm		
W_engines	18184		lbm		
W_nacelles & pylons	8112		lbm		
W_batteries	150		lbm		
SYSTEMS WEIGHTS		23927.2	lbm		
W_APU	400		lbm		
W_Instruments	4308		lbm		
W_Hydraulics	4789		lbm		
W_basic_electrical	3389		lbm		
W_avionics	2594		lbm		
W_furnishngs	5120		lbm		
W_airconditioner	3328		lbm		
TYPICAL RESIDUALS					
W_unusable_fuel	497		lbm		
W_oil	243		lbm		
W_pilots	350		lbm		
				MEW	196114 lbm
				BEW	201234 lbm
				OEW	202324 lbm
				MZFW	231764 lbm
				MLW	282100 lbm
				MTOW	399000 lbm
				Payload Weights	
				Commuter	24470 lbm
				Domestic	27670 lbm
				Long Haul	36055 lbm
				double check design payload!	

FIGURE 8 – Weight Estimation Spreadsheet

To estimate the design payload for this aircraft, we used the following regression from Takahashi [15]

$$PAYLOAD \geq (185 \cdot NPASS) + (30 \cdot 1.5 \cdot NPASS) \quad (1)$$

Which works out to a design payload of ~30,000-lbm for a 128-seat aircraft with all seats occupied and an average of 1.5 30-lbm checked bags per passenger. This is in-between the pro-forma weights for a domestic flight and the heavy checked bag expectations for economy class international customers.

B. Propulsion

Propulsion performance data, also known as five-column data has propulsion performance expressed in tabular form with net thrust and thrust-specific-fuel consumption (TSFC) as functions of speed (Mach), altitude (pressure altitude) and power setting (power-lever angle). The propulsion performance data in the supersonic engine files were given by

Professor Takahashi using NPSS [18] results have been post-processed to account for normal shock losses and "inlet buoyancy" as described by Takahashi & Cleary. [19] The basic performance was estimated using NASA's NPSS (Numerical propulsion system simulation), with the following assumptions: no shaft horsepower extraction, minimal engine bleed off-take, fan design point efficiency ~90 % at 5000 rpm low-pressure compressor (LPC) shaft speed, LPC and high-pressure compressor (HPC) design point efficiency ~88 % at 5000 rpm and 10000 rpm low-speed compressor (LSC) and high-speed compressor (HSC) shaft speeds, ~98 % adiabatic efficiency in the combustion chamber, low-pressure turbine (LPT) and high-pressure turbine (HPT) design point efficiency ~ 92 %.

The engines modeled represent a fundamental cycle evolved from, but otherwise not all that different from the old Pratt & Whitney JT8D-200 series turbofan found on an MD-80. [20] Engine models included a 1.0, a 1.5 and a 2.0:1 reference bypass ratio. All cycles had a reference Fan Pressure Ratio of 1.8:1, a normal shock inlet, with inlet diffusion commensurate to take the inflow from the capture area to the fan face. Reference OPR was 40:1. And maximum continuous power is associated with a 2900°R turbine inlet temperature. The engines have a small ~2% contraction from highlight-to-throat (i.e. A1.5 = 98% A1), but has substantial implied diffusion (A2 >> A1); see FIGURE 10.

Per ESDU [21], so long as the intake flow does not separate over the inlet lips, the additive drag balances the cowl lip suction; see FIGURE 10. So long as the inlet lips define the throat, we need not concern ourselves with the "buoyancy" effects of the implied contraction. Those forces are part of the cowl lip suction. At low speeds and high thrust settings, inlets are "under-sized" so that MFR>1; return to FIGURE 10.

Whereas at supersonic flight speeds, recall that the engine ingests air with a fan face Mach Number unlikely to exceed ~0.35. Therefore, a normal shock wave forms ahead of the cowl, trading velocity for pressure. Some post shock flow spills around the cowl; further diffusing and pressurizing. The remaining air flow, to enter the engine, will further increase in pressure as it diffuses within the inlet; see FIGURE 11.

Turning to FIGURE 12, we can see that the diffuser substantially pressurizes the inlet duct. At MFR~75%, the inlet buoyancy offsets between 10% and 22% of the

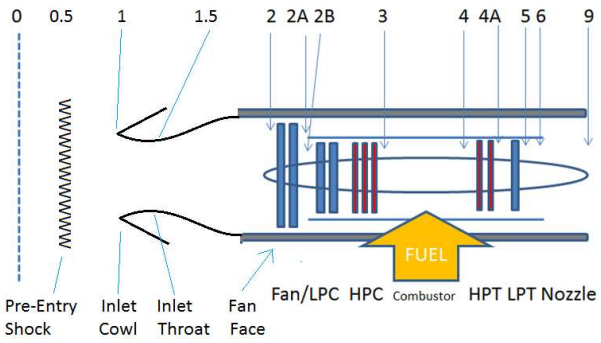

FIGURE 9 – Expanded Station Nomenclature Used Here

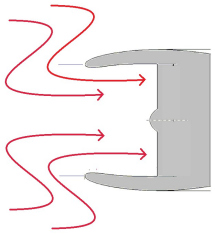

FIGURE 10. Subsonic Operation at MFR>1; Reverse Flow around the Cowl Lip.

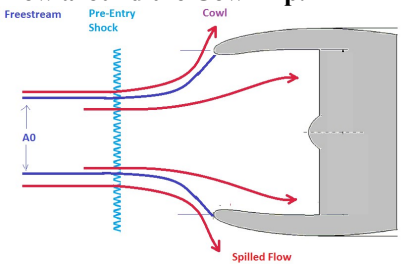

FIGURE 11. Supersonic Operation at MFR<1; Swallowed flow experiences shock wave upstream of inlet cowl and further diffuses before reaching the cowl.

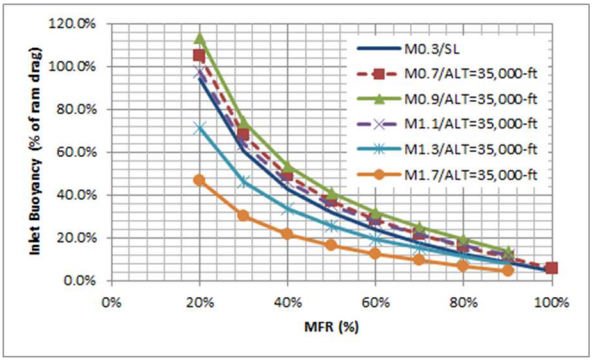

FIGURE 12. Inlet Buoyancy (% of ram drag) as a Function of MFR for various flight conditions. Inlet diffusion ratio as found on an F-18A [19]

total ram drag. As the inlet MFR declines, the inlet pressurizes more strongly while the ram drag falls off. Hence, at the lowest computed MFR, the inlet buoyancy may actually exceed the ram drag of the swallowed flow.

All of these corrections, customized for the engine / inlet pairings at hand, have been folded into the "installed five-column-data" used for this design study. This study quickly settled on using engine data scaled to ~45,000-lbf sea-level, static thrust.

C. Aerodynamics

VORLAX is a vortex lattice CFD code that the team used to produce stability & control aerodynamic data. [22] We modelled the aircraft as a series of flat plates - to calculate *CL*, *CDi* and the various stability derivatives. Control surfaces were included in the model and deflected in order to estimate control power from the ailerons, rudder and elevator.

EDET is an Empirical Drag Estimation Technique (*EDET*) used to estimate zero-lift friction, zero-lift-wave drag and "trimmed" performance data. [23] It works by inputting the various dimensions of the aircraft from the fuselage length, fuselage area, wing span, wing wetted area, as well as the characteristics of the vertical and horizontal tail. *EDET* uses a semi-empirical method to estimate total drag from the following build up:

$$CD(CL, M, ALT) = CD_{skinf}(M, ALT) + CD_{base}(M, ALT) + CD_c(M, ALT) + CD_{crud} + \frac{CL^2}{AR} + CD_p(CL, M) \qquad (2)$$

Where *CDc* is an estimate of zero-lift compressibility drag and *CDp* is an estimate of lift-dependent "non-parabolic" drag, that includes "wave-drag-due-to-lift."

Because of the nature of supersonic aircraft, it is beneficial to have thinner swept wings and a slender fuselage. This is because of the supersonic regime, and the pressure drag due to the shock waves that form as a result. For these reasons, to minimize the effects of shock waves, the wing had to be thin and swept.

The *EDET* supersonic data tables are limited to wings with $t/c < 6.5\%$. While this *t/c* ratio is beneficial for supersonic flight, however it can have negative effects on maximum lift coefficient, structural mass and fuel volume.

The fuel requirements were integrated along the wing in the wing thickness tool, giving accurate data of the area required for fuel storage. In order to solve this problem of having a thin wing that would need fuel to be somewhere inside, the chord length was increased to allow for greater volume for fuel storage.

D. Point Performance

In order to estimate the aircraft performance over a large area of varying altitudes and Mach numbers, a "sky map" tool was developed. [14][24] Sky map contour plots of aircraft performance as a function of Mach and altitude for a given flight weight are based on two key inputs: the *EDET* output file and a 5-column propulsion data file.

Skymap gave the team an estimate for how the aircraft would perform during flight operations.

For initial data estimations, the weight was set to that of a Concorde, with 400,000 pounds and an engine factor of 30 (~170,000-lbf total sea-level-static thrust).

With this data, key characteristics of the aircraft could be found such as the coefficient of lift, as well as lift and drag.

$$C_L = \frac{W}{q * S_{ref}} \qquad (3)$$

$$D = C_D(M, CL, ALT) * q * S_{ref} \qquad (4)$$

With the use of the propulsion input file, the cruise fuel flow (FF) could be found.

$$FF = TSFC * D \tag{5}$$

For climb, we consider the specific excess thrust (SET), with the engines set to full power:

$$SET = \frac{T_{max} - D}{W} \tag{6}$$

We can also estimate the flight speeds of knots true airspeed (KTAS) and knots indicated (equivalent) airspeed (KEAS) to finally predict the unaccelerated rate of climb (ROC):

$$KTAS = M * a * 3600/6080 \tag{7}$$

$$KEAS = 660.8\sqrt{\frac{q}{1481 lbf/ft^2}} \tag{8}$$

$$ROCu = SET * KTAS * 101.33 \tag{9}$$

In order to understand fuel efficiency, we need to compute Specific Range. The most efficient flight will occur at the altitude and speed with the highest *SR*:

$$SR = \frac{KTAS}{FF} \tag{10}$$

As it can be seen, *SR* is dependent on the KTAS of the aircraft and the fuel flow, which is an indirect function of speed, altitude and weight.

The data collected from this skymap tool would be used in our mission file, as the sky map would provide data for the best cruise Mach (BCM) and best cruise altitudes (BCA) that we would be flying at. This is crucial as it would ensure that the mission the aircraft would take, from takeoff to landing would be based on what altitude and speed would result in the best performance.

E. Mission Performance

In order to predict the overall aircraft performance, we used a point-mass-simulation mission performance tool. [15] This tool only required three inputs in the form of an aerodynamics file taken from *EDET*, a 5 column engine file that contained data on the engine used, and a mission input file. This mission input file would describe a typical flight, from climb speed, distances flown, all the way from takeoff to landing. The aerodynamics and propulsion file are determined based on the specific range constraints from the sky maps tool.

While the mission file can be modified to behave however we want the flight plan to be, there are two key regulations that have to be kept in mind. These were the speed limit of 250 KEAS under 10,000 feet which is described in 14 CFR § 91.117 “Aircraft Speed”, but also 14 CFR § 91.817 “Civil Aircraft Sonic Boom”, which prohibits sonic boom over land, meaning that a Mach Number greater than 1, can only be achieved over the ocean. [8] These two regulations cannot be modified, and had to be incorporated into the mission plan.

The first phase of flight is takeoff, which as described earlier has a speed limit under 10,000 feet.

In order to determine the en-route climb speed, we analyzed the sky maps for the best performance. For the final design, we determined initial heavy weight subsonic cruise at M 0.86 around 20,000-ft.

For the major portion of the flight, over water, the aircraft will accelerate and climb to its supersonic cruise point. For the final design, we found best performance at a cruise altitude around 40,000-ft. The relatively low cruise altitude and speed, compared to Concorde, was a byproduct of the strong altitude and speed lapse of thrust from the normal shock inlet equipped turbofan engines needed to achieve reasonable cruise efficiency within modern take-off and landing noise constraints.

Subsonic final cruise, descent and landing are all modelled with the point-mass simulation using speed profiles determined using the "sky maps" point performance code.

F. Takeoff & Landing

The team developed a takeoff and landing performance tool in order to see how long the runway has to be for a supersonic aircraft to safely depart from an airport. The analysis of runway length and takeoff speed were conducted several times to make sure that the designed aircraft can land within the limit of runway length of the major airport in the flight route.

Initial predictions were made using Roskam's empirical formula: [15][25]

$$CFL = 37.5 * \frac{(W/S_{ref})}{CL_{max}*(T/W)} \tag{11}$$

CLmax will be the lift coefficient with flaps deployed at takeoff, and W is maximum takeoff weight.

Along the way, we realized a number of issues stemming from this purely statistical approach.

Our final performance estimates are produced using Takahashi's time-step-integrating takeoff code; this is discussed in greater detail in his text [25] and in a companion paper published at the 2021 AIAA SciTech conference [26].

In addition, for the takeoff, the performance tool computes the takeoff safety speed, *V2*, based on the stall speed at takeoff :

$$Vs = \sqrt{\frac{(W/S_{ref})}{1481CLmax}} \tag{12}$$

$$V2 = max(1.13Vs, 1.1VMCA) \tag{13}$$

VMCA is computed using the stability & control tool populated by *VORLAX* aerodynamic data.

The simulation also gives the % climb gradient of aircraft, assuming the small angles:

$$\%\, Gradient = \frac{T - C_D q S_{ref}}{W} * 100 \tag{14}$$

For the landing configuration, our tool estimates the final approach speed, *VREF*, where landing flaps are deployed and gears are extended, and landing distance required.

In order to understand landing distances, *VREF* needs to be calculated first using Vs in landing configuration and minimum control landing speed, *VMCL*.

$$V_{ref} = max(1.23Vs, VMCL) \tag{15}$$

We initially used Roskam's estimate cues for the basic landing distance (*LDR*) as a function of the *VREF* speed: [15][25]

$$LDR = 0.3 * {V_{ref}}^2 \tag{16}$$

When dispatch planners consider the legal landing distance required for an aircraft, they often refer to the landing distance factored by 1.67 for 14 CFR § 121.195 compliance.

$$LDA > 1.67 * LDR \tag{17}$$

As with takeoff, we realized a number of issues stemming from this purely statistical approach.

Our final performance estimates are produced using Takahashi's time-step-integrating landing code; this is discussed in greater detail in his text [25] and in the companion paper published at the 2021 AIAA SciTech conference [26].

G. Stability and Control

The team built a Stability & Control screening tool to understand the behavior of candidate airframes. This tool uses *VORLAX* to model the controls neutral airframe in pitch and yaw and models a zero-sideslip angle airframe in pitch with various control surfaces deflected.

We design the aircraft to be statically stable, without the need for complex stability augmentation systems at any speed. Thus, across the entire envelope:

$$\frac{dCn}{d\beta}(M, \alpha) > 0 \tag{18}$$

$$\frac{dCl}{d\beta}(M, \alpha) < 0 \tag{19}$$

$$\frac{dCm}{da}(M, \alpha) < 0 \tag{20}$$

To set the static margin, we use MIL 8785C screening criteria. [27] This standard provides guidelines for stick-fixed short period frequencies as a function of pitch responsiveness. We estimate short period frequency as:

$$\omega_{sp} = \left(\frac{1}{2\pi}\right) * \sqrt{\frac{-57.4*\left(\frac{dC_m}{d\alpha}\right)*q*SREF*\underline{c}}{I_{yy}}} \tag{21}$$

and the pitch responsiveness as:

$$\frac{n}{\alpha} = \frac{57.4 * q * Sref * \frac{dC_L}{d\alpha}}{W} \tag{22}$$

We use the MIL STD 8785C guideline for "Category C" flight phases to set the static margin. Our aircraft is in the "Level 1" zone, which assures that flying qualities are entirely adequate for the flight regime.

Cnβdynamic represents the yawing and rolling moments weighted by the ratio between the yawing mass moment of inertia (*Izz*) and the rolling mass moment of inertia (*Ixx*). [15]

$$C_n\beta\ Dynamic = \frac{dCn\ Body}{d\beta} * cos\ \alpha - \frac{d\ Cl\ body}{d\beta} * \frac{I_{zz}}{Ixx} * sin\ \alpha \tag{23}$$

Where the Dutch Roll frequency can be estimated as: [15]

$$\omega_{dr} = \left(\frac{1}{2\pi}\right) * \sqrt{\frac{-57.4 * Cn\beta\ Dynamic * q * SREF * \underline{c}}{I_{zz}}} \tag{24}$$

Lateral control departure parameter measures the extent of coupling between the roll and yaw effects of the ailerons and the inherent lateral and directional stability of an airframe.

$$LCDP = \frac{d\ Cn}{d\ \beta} - \frac{dCl}{d\beta} * \frac{\frac{d\ Cn}{d\ ail}}{\frac{d\ Cl}{d\ ail}} \tag{25}$$

Once these values are computed, we can cross-plot these parameters on a Bihrle-Weissman Chart. Basically, we want to design the aircraft to have a stable Dutch Roll (*Cnβdynamic* > 0) and favorable aileron control (*LCDP*>0) to be departure and spin resistant.

V. Trade Studies Supporting the Final Design and Optimization Strategies

It is imperative that when designing an aircraft we consider how the independent design variables affect key performance parameters and vice versa. The tools mentioned above need to be combined in order to effectively iterate through designs and trade studies. This is where analysis tools like *ModelCenter* are useful; see FIGURE 13. This tool allows us to change specific design parameters (such as wing sweep) in order to get the best possible design that meets the requirements.

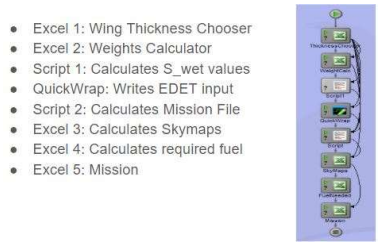

FIGURE 13: *ModelCenter* tool

A. Fuselage and Interior Layout

For the fuselage design, what needs to be considered is that there needs to be enough room for both cabin and luggage. The fuselage diameter is set large enough so that each passenger can have one large (or two small) checked baggage.

In order to determine the number of seats, the team researched the transatlantic premium seating market capacity in the fall of 2019. For example, looking at Delta Airlines flights between Atlanta and Amsterdam, which are major airports used for the designed flight routes, we realized that the market supports an average of 128 premium passengers per day. Therefore, we sized our aircraft to feature an interior with 32 rows of four abreast (2+2) "domestic daylight route" business class seats, each with a 20-inch width and 35-inch pitch; see FIGURE 14.

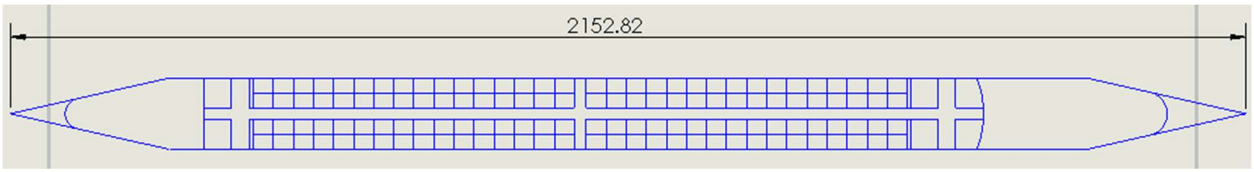

FIGURE 14: Interior Layout

To comply with 14 CFR § 25.815 and 14 CFR § 25.803, the aisle width is 20 inches; there are two type B doors in the front, two type III hatches in the middle, and two type C doors in the back of the interior. There is one lavatory and kitchen in the front of the aircraft and two lavatories and kitchens in the back. The lavatories and kitchens are 3 feet by 4 feet and the cockpit size is similar to that of a Boeing 767 and 777 that typically fly the same Trans-Atlantic routes.

Since the fuselage tube is too narrow to support underfloor baggage, behind the aft bulkhead we grant 20 feet of additional fuselage length for passenger baggage.

We tinkered with the idea of a 3-across layout but ultimately decided on 4-across. With a 3-across layout and 128 premium passenger seats, the fuselage would be much longer and narrower. There would not be enough storage space below the cabin for fuel and baggage. A 4-across layout shortened the fuselage without making the diameter that much wider. Additionally, a 4-across layout was symmetric and seemed less 'awkward'.

The nose is based on a conical form with a 12.5-deg semi-vertex angle in order to not cause a detached shock at speeds greater than or equal to Mach 1. [28]

Thus, our fuselage is 180 feet long, 123 inches in diameter and has 7 feet of interior passenger standing room; see FIGURE 15.

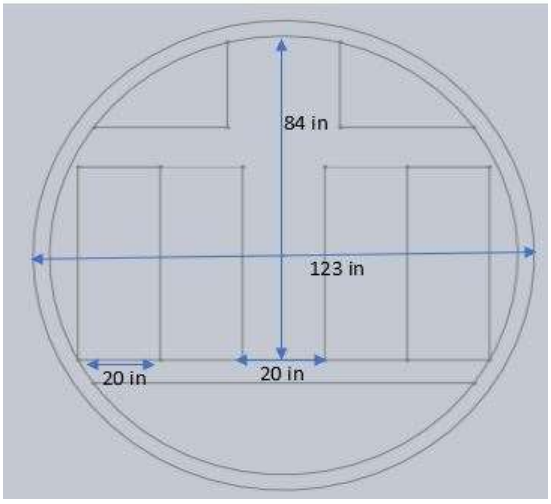

FIGURE 15: Interior Cross Section

B. Overall Vehicle Design

As shown in FIGURE 13, we used *ModelCenter* to link the tools we built to conduct trade studies in order to optimize our design. The tools used for the trade studies include the wing thickness chooser, weights calculator and Skymaps generator.

We made a script that calculated the wetted wing area using data from the wing thickness chooser. The *EDET* data is then generated using the *QuickWrap* feature in *ModelCenter*. Another script was made that calculates the Mission File, which then produces the Skymaps. We can then obtain the required fuel for the mission and compare it to the maximum fuel our plane can carry.

The key parameter we needed to optimize was our specific range (*SR*); this parameter measures the efficiency of our plane. We started by approximating the geometry and weights and ran *ModelCenter* with each propulsion file. From that. we recorded the maximum *SR* at Mach 0.86 (Subsonic cruise), 1.2 and 1.4 (Supercruise) for each propulsion file. This tells us which engine produces the best *SR*. After choosing the best engine, we can vary other parameters (using the same process) such as sweep, *SREF* and *t/c* to optimize our wing design.

C. Wing Design

The overall wing size and configuration is driven by several factors: 1) supersonic cruise aerodynamic efficiency, 2) takeoff performance, 3) landing performance, 4) structural weight and 5) fuel capacity. For this aircraft, we found that the main factor driving wing design was fuel capacity.

To estimate fuel capacity, we integrated the volume displaced by a viable torque-box region comprising 50% of the chord of the basic trapezoidal planform and 70% off the local thickness. As we changed design parameters, like *Sref*, span (b), taper ratio (TR), Yehudi size and the design Mach/Altitude/Weight, we ensured that our proposed design could provide the fuel capacity needed to fly the mission.

The Korn equation [29] controls the interplay between design *CL*, design Mach, *t/c* ratio and sweep for shock formation related drag divergence.

$$M_{dd} \approx M_{cr} + 0.05 \approx \left(k + 0.1\, CL_{design} + \left(\frac{t}{c}\right)\right) + 0.05$$

We implemented the swept wing Korn Equation [15] across the wing-span as a thickness choosing tool (see FIGURE 16):

$$\frac{t}{c}(span) = k\cos(\Lambda) - 0.1\,Cl(span) - (M_{des} - 0.05)\cos^2(\Lambda)$$

Where $k \sim 0.82$.

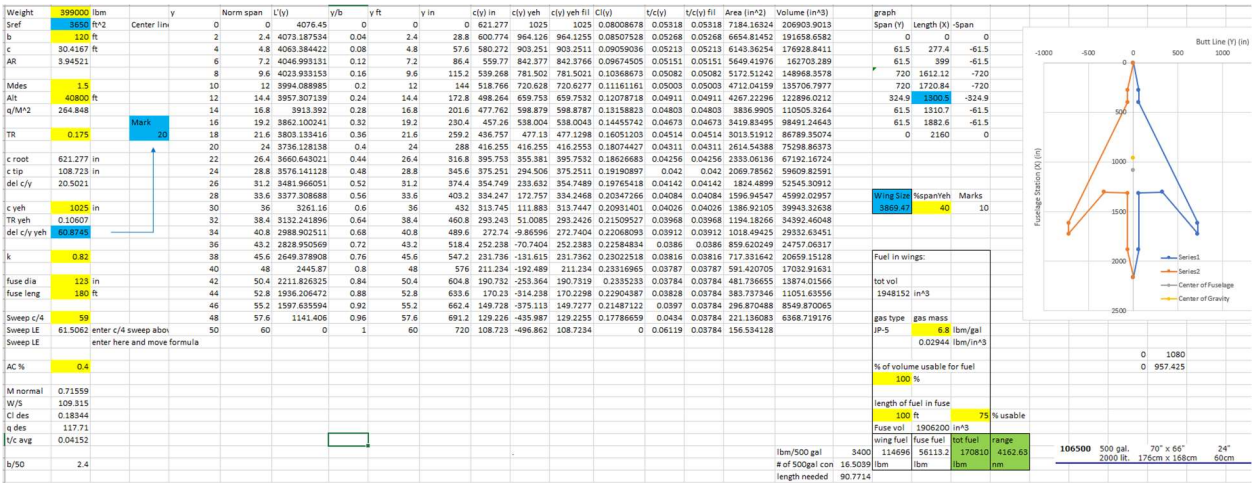

FIGURE 16: Wing Thickness Chooser

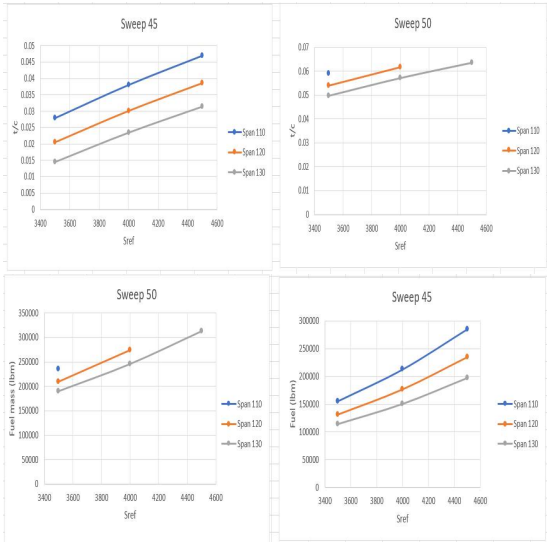

FIGURE 17: Example of trade study varying Sweep,*Sref* and Span

Another factor of wing design was the thickness to chord ratio. Not only did we have to keep this low in order to reduce shock formation, but we also had to keep the average < 6.5% to utilize the *EDET* wave drag tables.

We performed deep trade studies to determine the optimum wing configuration. For example, making *TR* low (highly tapered wingtips) allows us to hold a decent amount of fuel, but compromises stall characteristics. Increased sweep permits a thicker *t/c*, which allows more fuel, but we needed to keep it within reason to keep the mean *t/c*< 6.5%. And wing sweep and aspect ratio had an unexpected interplay; as we swept the wings more, we had to decrease span in order to avoid striking a wing tip on takeoff or landing.

The trade studies conducted gave us a wing that fulfilled our fuel, *SR* and field performance requirements. We wanted to maximize our fuel capacity while minimizing our wing thickness. This is so that our plane would have the range capable of transatlantic flight while sustaining supersonic speeds. With our tools connected, it was only a matter of varying sweep, *Sref* and span; see FIGURE 17.

Initially, we used two different sweep angles, three different *Sref* values and three different span values for our trade

studies. Once we ran the numbers, we compared the *t/c*, *SR* and Fuel Capacity to determine the best combination. Our final wing features a span of 120 feet, a quarter chord sweep of 59 degrees, an *AR* of 4.114, a *TR* of 0.3 and a *Sref* of 3650 sq.-ft. This wing has the lowest possible *t/c* with the highest possible fuel capacity and *SR* that meets the range requirements.

Fuel is being stored in the wings and in the fuselage in the region of the wing / body junction. The fuel in the wing totals ~115,000-lbm, while the undercarriage of the fuselage holds ~56,000-lbm. The fuel in the wing will be held inside the torque box. The approximation for this volume was calculated at 0.7 of the thickness and 0.5 of the chord at each location, and then integrated along the span. The fuel in the fuselage will be held inside portioned fuel bladders. The dimension of these fuel bladders are 70 in by 66 in and a max height of 24-in. These dimensions are able to easily fit in the bottom of the fuselage. Each bladder will hold 500 gallons of fuel. The separation of fuel into smaller volumes will also help with fuel slosh, acting to minimize the distance the fuel can move and keeping the fuel distributed across the CG. The length of fuselage that will be holding fuel is approximately 100-ft.

Matching our fuel, *t/c,* and payload requirements, we were able to get an ideal wing design; see FIGUREs 18 and 19. The fuel capacity, which was a major driving force in the wing design. The overall fuel capacity is ~171,000-lbm, which closely aligns with the fuel requirements defined by the sizing mission (see Section II). The wing has a trapezoidal planform area that leads to *Sref*=3,650-sq.ft.; the inboard portion of the planform includes a large "yehudi" for flap and landing gear integration. The wingspan, tip-to-tip is 120-ft. The wing quarter chord sweep is 59-deg. The wing leading edge sweep is 61.5-deg. The wing thickness varies from ~5.5% at the side of body to ~4.0% outboard; this is consistent with other low-supersonic aircraft like the F-18 fighter.

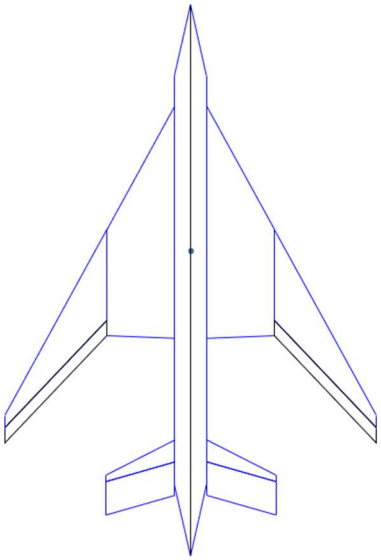

FIGURE 18 - Wing Planform

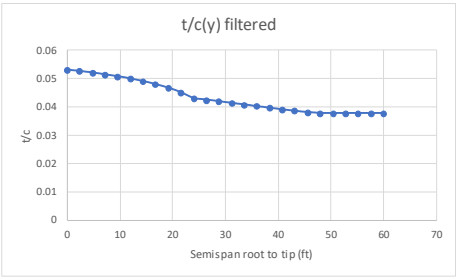

FIGURE 19 – *t/c* as a function of span plot

We can see that the Mach number of the flow normal to the leading edge is clearly subsonic: $M\cos(\Lambda_{LE}) = 1.5\cos(61.5^o) = 0.72$. This substantiates the use of the Korn equation to select thin, but otherwise conventional (i.e. NACA 4-digit "teardrop") forms for the defining airfoils.

The wing "yehudi" is needed to integrate the main landing gear. The aircraft needs to rotate to a considerable angle of attack during takeoff and landing. It is a simple geometry problem to calculate the landing gear height needed so that tail strike would not be a possibility. In order to calculate the landing gear height, the distance from the rear gear to the end of the aircraft, as well as the takeoff angle of attack needed to be accounted for. Because these were measured values the process was straightforward, and the landing gear was found to be 11.39 feet tall.

With the maximum takeoff weight of 399,000-lbm, the team decided to use a total of 12 tires (6 tires per bogey) for the main gear; see FIGURE 20 (overleaf). Based on our takeoff and landing analysis, the takeoff safety speed, *V2*, at *MTOW* is ~ 183 KEAS, which is equivalent to about 211 miles per hour. With those required rated load and speed, we specify a pair of 18x5.7-8 250-mph rated tires for the nose wheel, and 36x11.0-18 rated at 227 miles per hour for the main gear. The main wheel tires have a rated load of 35,880-lbf, which just exceeds the 1.07 load-rating factor-of-safety specified in 14 CFR § 25.735.

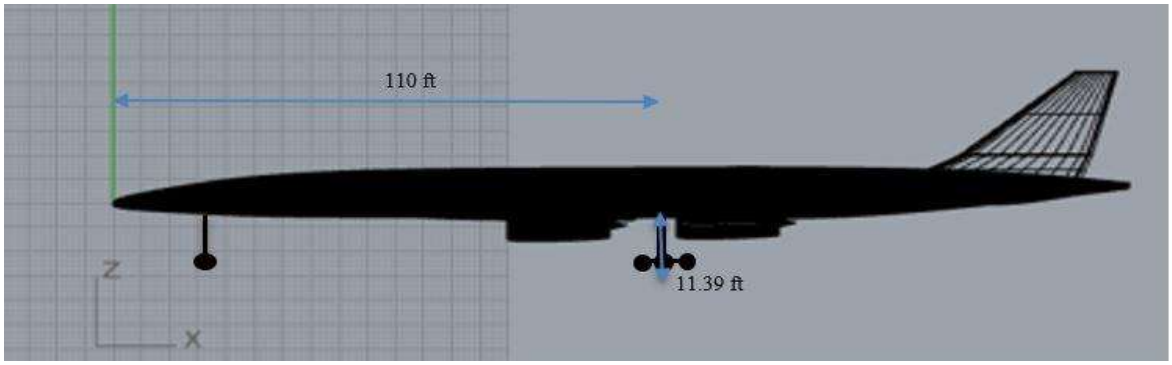

FIGURE 20 – Position and height of main landing gear

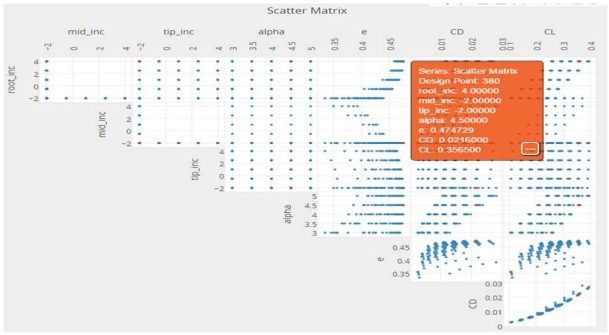

FIGURE 21: Wing Twist Trade Study

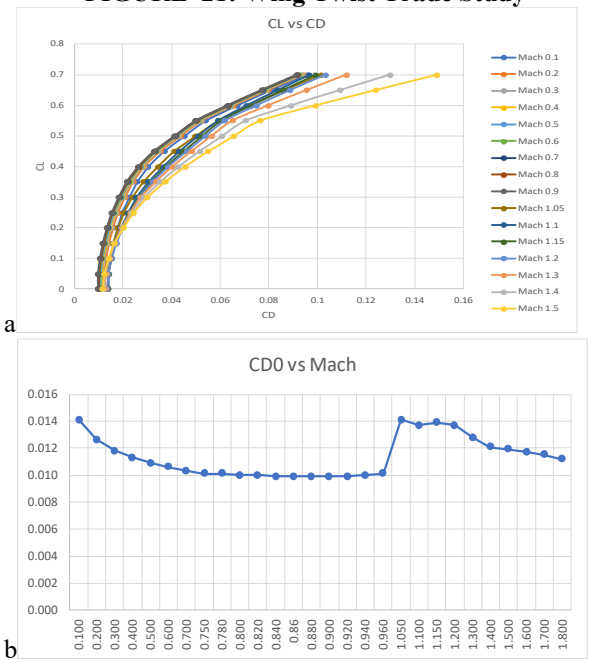

FIGURE 22: *EDET* drag polars. a) CL vs CD, b) CD0 vs MACH #

We used *VORLAX* in conjunction with *ModelCenter* to optimize the twist of the wing. To run this trade study, we modelled the aircraft in terms of a fuselage and the wing planform with several midspan control points. *ModelCenter* could then vary both the angle-of-attack of the entire aircraft as well as the wash-in or wash-out of the wing at the side-of-body, mid-span and wingtip. We then varied all of these design variables to determine the twist distribution that gave us the lowest possible induced drag at the design lift coefficient. The study was run to maximize elliptical distribution by varying the tip, mid, and root incidences. The minimum induced drag at our cruise design CL (*CL~0.36*) was found with the fuselage at 4.5-deg angle-of-attack, the wing root incident at at +4-deg (wash in) and the mid and tip incidence at -2-deg (wash out); see FIGURE 21.

FIGURE 22 shows our drag polar as well as zero-lift drag vs. Mach number. These plots were generated using our *EDET* tool. [23] The drag polar plot (FIGURE 22a) shows the aerodynamic efficiency at different speeds at which the aircraft is flying. The drag coefficient is highest at ~0.35 when the aircraft is cruising at Mach 1.5.

FIGURE 22b shows the zero-lift drag as Mach number increases. There is a sudden increase in drag as Mach exceeds 0.95. This would be where the critical Mach number is for our aircraft. The critical Mach number occurs when the air moving over any point of the wing is equal to Mach 1.

D. Engines

In order to avoid ETOPS problems, and to allow for a smaller vertical tail for engine-out trim, the team

1.0	4-1
TERMINATION	1
Winit	350000
Wfinal	205442.719
Wmin	188066
Total Mission Time	27013
Total Dist Flown	4969.86787
Credit Dist	4835.4707
Time in Loiter	0
Excess Payload	17376.7188
Fuel Burned	144557.113
Credit Fuel	139752.628
Total ESAD Flown	4969.8999

1.5	4-1
TERMINATION	1
Winit	350000
Wfinal	212789.578
Wmin	188066
Total Mission Time	27049
Total Dist Flown	4963.11382
Credit Dist	4828.58008
Time in Loiter	0
Excess Payload	24723.5781
Fuel Burned	137210.511
Credit Fuel	132367.77
Total ESAD Flown	4963.10986

2.0	4-1
TERMINATION	1
Winit	350000
Wfinal	196121.656
Wmin	188066
Total Mission Time	26907
Total Dist Flown	4960.50019
Credit Dist	4826.66895
Time in Loiter	0
Excess Payload	8055.65625
Fuel Burned	153878.468
Credit Fuel	149023.154
Total ESAD Flown	4960.52832

1.5	5-1
TERMINATION	1
Winit	350000
Wfinal	189743.672
Wmin	188066
Total Mission Time	26850
Total Dist Flown	4950.24601
Credit Dist	4816.59277
Time in Loiter	0
Excess Payload	1677.67188
Fuel Burned	160255.869
Credit Fuel	155639.885
Total ESAD Flown	4950.24609

1.0	6-1
TERMINATION	0
Winit	350000
Wfinal	187945.359
Wmin	188066
Total Mission Time	17872
Total Dist Flown	3745.1273
Credit Dist	3745.90942
Time in Loiter	0
Excess Payload	-120.64063
Fuel Burned	162054.807
Credit Fuel	162054.807
Total ESAD Flown	3745.1167

1.5	6-1
TERMINATION	0
Winit	350000
Wfinal	188039.141
Wmin	188066
Total Mission Time	19000
Total Dist Flown	3998.24825
Credit Dist	3999.02954
Time in Loiter	0
Excess Payload	-26.859375
Fuel Burned	161960.787
Credit Fuel	161960.787
Total ESAD Flown	3998.25439

2.0	6-1
TERMINATION	0
Winit	350000
Wfinal	187775.594
Wmin	188066
Total Mission Time	16813
Total Dist Flown	3510.71508
Credit Dist	3511.50195
Time in Loiter	0
Excess Payload	-290.40625
Fuel Burned	162224.543
Credit Fuel	162224.543
Total ESAD Flown	3510.71973

FIGURE 23: Engine BPR / Inlet Sizing Trade Study

decided early on a four-engine layout with the normal-shock inlet engines slung underneath the wing with the inlets positioned far in front of the leading edge.

We used the point-performance "Skymap" code to explore which engine configuration (bypass ratio and inlet size) would provide the best performance at our Mach numbers and altitudes of interest. Because our defining variable was specific range, it was easy to filter out the maximum specific range that each engine provided and compare them.

FIGURE 23 shows a trade-study matrix where we examined seven candidate engine cycles to pick an optimum for our mission. We considered BPR 1.0, 1.5 and 2.0 engines with small inlets, a BPR 1.5 engine with a medium sized inlet and BPR 1.0, 1.5 and 2.0 engines with larger inlets. For a Mach 1.5 cruise mission aircraft, we found the minimum fuel burn to be associated with the BPR 1.5 engine with the smallest proposed inlet – this configuration balances the thrust lapse with increasing speed and altitude from the higher bypass ratio against the "inlet buoyancy" effects from the inlet diffusion that mitigates against ram drag. [19]

E. Mission Optimization

In order to properly size this aircraft, it is important to define the sizing mission not only in terms of its equivalent still air range (ESAD), but in terms of the relative proportions of subsonic and supersonic flight; refer to Section II for a deeper discussion of the market drivers (ATL to AMS and return) for the "design mission." Using all the data collected, the flight ESAD could be found for the longest east to west flight (Europe to North American). Thus, we ended up with the following virtual "flight plan." (refer back to FIGURE 3 in Section II).

The aircraft departs Amsterdam and climbs to 10,000-ft under the regulated 250 KEAS. From there it speeds up to Mach 0.7 and climbs to FL200 (20,000 ft). It flies the first, subsonic leg at M 0.86 for approximately 400-NM until it clears the UK. From there, it climbs up and accelerates to its heavy weight optimum supersonic cruise point at Mach 1.5 at FL450 (45,000-ft). As the aircraft burns off fuel, it step-climbs to FL500 (50,000-ft). As the aircraft nears Atlanta, off the Carolina coast it decelerates and descents to M 0.86 and FL220 (22,000-ft) to fly the last 400-NM over land. As it nears Atlanta, it further slows and descends for arrival; see FIGURE 24.

The sizing mission also includes a balked landing, subsonic climb back up to 10,000 ft, flies the necessary 150-NM diversion to an alternate (i.e. Charlotte, NC) and finally descends for landing.

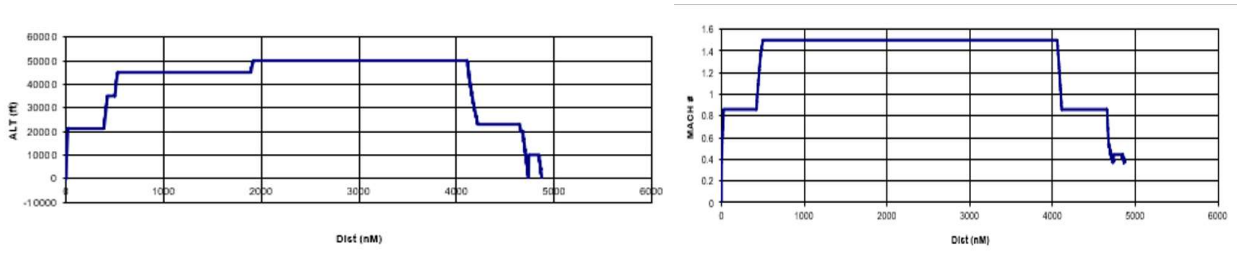

FIGURE 24 – Sizing Mission Flyout

TERMINATION	1
Winit	399000
Wfinal	232109.1406
Wmin	202369
Total Mission Time	25083
Total Dist Flown	4872.719541
Credit Dist	4738.293945
Time in Loiter	0
Excess Payload	29740.14063
Fuel Burned	166891.6055
Credit Fuel	161462.277
Total ESAD Flown	4872.710938

FIGURE 25 - Mission Code Output

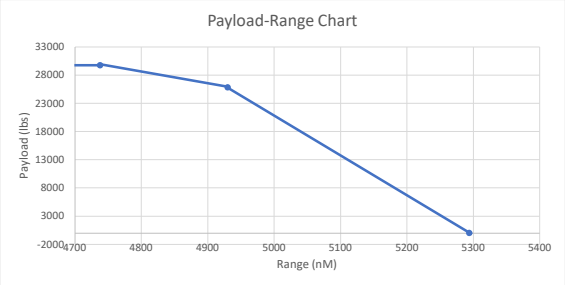

FIGURE 26: PAYLOAD / RANGE CHART

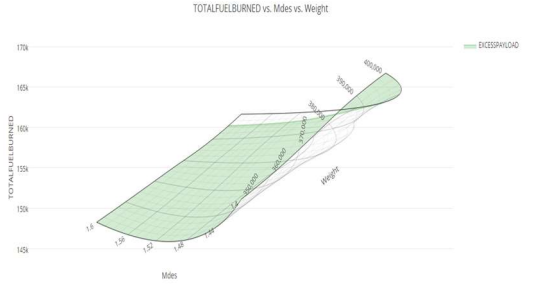

FIGURE 27: Mdes vs Payload Trade

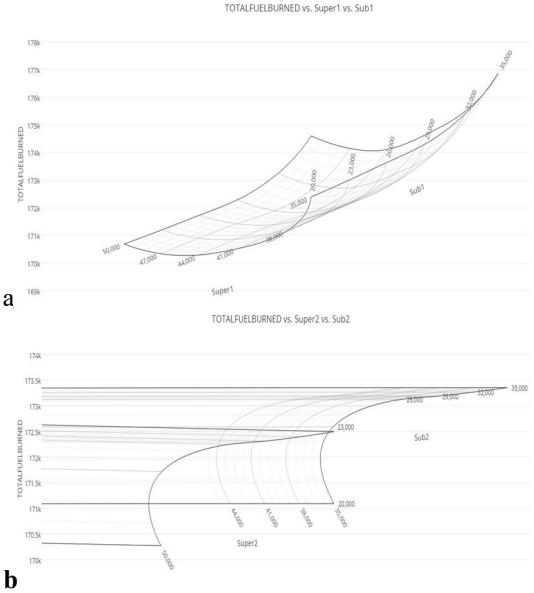

a

b

FIGURE 28: Fuel Burn vs Cruise

Using this worst-case ESAD data, we sized the aircraft for ~4,730-NM "credit distance" still-air flights; with 6 hours and 50 minutes aloft; see FIGURE 25. This sets a design maximum takeoff weight of 399,000-lbm and an *OEW* ~ 202,000-lbm for an aircraft with a predicted fuel burn of ~161,500-lbm holding ~5,500-lbm fuel in reserve with an economic payload of ~29,750-lbm. Since the wing can hold ~114,696-lbm of fuel within the torque box, we see how we drove the wing size by the fuel capacity needed to fly the mission

The payload range chart was made with the help of our mission code; see FIGURE 26. We ran 3 cases, 1) Max payload at *MTOW*, 2) Max fuel at *MTOW* and 3) Max fuel with no payload, landing at *OEW*. With our aircraft fully loaded and fueled, it can achieve a range of 4,730-NM "credit distance". The second case, with a tradeable value in payload for maximum fuel achieved a range of 4930-NM. The third case, with no payload and landing at *OEW* achieved a range of 5294-NM. At cruise speed and altitude, we achieve a specific range of 0.031-NM/lbm, which is like the Concorde's (0.0326-NM/lbm). Compared to the all business class A318 which has a fuel burn per seat of 0.0769 lbm/NM/seat, the ***Atlantic Shuttle*** is reasonably efficient at 0.268 lbm/NM/seat. For a routine trip from AMS to ATL (4596-NM) the ***Atlantic Shuttle*** would cost roughly $541.96 in jet fuel per seat.

The team decided upon the Mach 1.5 cruise point as a result of extensive trade studies, several which will be showcased here. Turn to FIGURE 27 to see the result of a coupled trade study performed using the full *ModelCenter* integrated model. We varied the design Mach number and design flight weight for supersonic cruise (together they directly define the wing thickness – and indirectly drag and fuel capacity) to find the most economical design. We see in FIGURE 27 that the minimum fuel burn occurs with a wing designed for and supersonic flight operated at Mach 1.5.

Turn next to FIGURE 28, where you can see how we optimized our flight profile for the lowest fuel burn numbers, while keeping the constraint for payload at range. Here in FIGURE 28a, we plot the fuel burn as a function of initial subsonic cruise altitude (Sub1 varied from FL200 to FL350) and initial supersonic cruise altitude (Super1 varied from FL350 to FL500). Moving to FIGURE 28b, we plot the fuel burn as a function of supersonic cruise-climb altitude (Super2 varied from FL350 to FL500) and final subsonic cruise (Sub2 varied from FL200 to FL350). Together they define the surprisingly low altitudes for subsonic flight (FL200 to FL220) and large step-climb (5,000-ft) featured in the final

sizing mission. The large step change between the first supersonic and the second supersonic is due to a decrease in weight as fuel is burned off, allowing the plane to increase in altitude to get a more ideal *SR*. Even more fuel could be saved if air traffic control were to permit continuous cruise-climbs instead of step-climbs as they did with Concorde [31].

F. Stability and Control

Stability & Control governs the final aerodynamic configuration. The team varied wing dihedral, tail size, control surface size and deflection, and center of gravity location to get desirable static and dynamic stabilities, engine-out trim capability, crosswind trim capability as well as obtaining favorable Bihrle-Weissman spin resistance. [15][30] The highly swept wing inherently develops a very strong dihedral effect, which rises with increasing angle-of-attack; while dihedral-effect is desired, too much of a good thing is detrimental to other stability & control issues.

We found that the geometric wing dihedral is a major contributor to $dCl/d\beta$; varying it allowed us to trade crosswind trim capabilities against dynamic stability.

The vertical tail size contributes to weathercock stability; its size also contributes to getting the design into the "A" region of the Bihrle-Weissman chart. [30]

The control surface sizing is used to establish necessary trim in pitch, roll and yaw. The aircraft needs a lot of elevator control power; an all flying horizontal tail.

The center of gravity manipulation allowed us to adjust the static margin which controls both the short-period-frequency and has an effect on elevator trim as well; see FIGURE 29. We began our design with a nominal CG placed 45% of the way along the fuselage; we refined the CG location to balance the static margin (hence, short period), the distance from the landing gear to the CG (and hence the Yehudi size), and in turn the trim of the plane; see FIGURE 30. It was particularly important to manipulate where our main landing gear is in relation to the center of gravity and the aerodynamic center to help in takeoff and landing.

The mass moments of inertia used to estimate the short-period and Dutch-Roll frequencies are computed using Roskam's empirical equations [15][31]; see FIGURE 31.

While we looked at the effects of dihedral and anhedral, in the end we chose a wing with zero geometric dihedral as a compromise between dynamic stability, crosswind capability and wingtip strike. As a result, our ailerons are

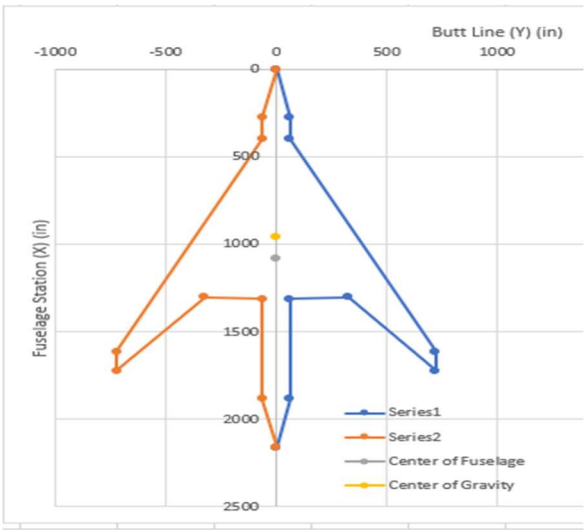

FIGURE 29 - Wing / CG placement on fuselage

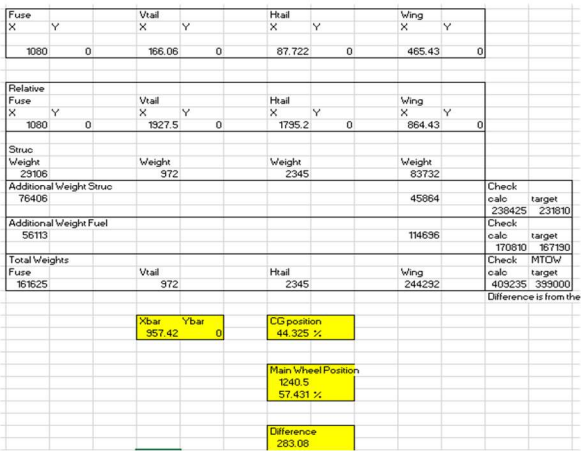

FIGURE 30 - CG placement tool

Mass		Wing	
Weight	399000	Sref	3650
Ixx	10324871	AR	3.945205
Iyy	15706300	b	120
Izz	2617035.3	c	30.41667

FIGURE 31 - Estimated Mass Moments of Inertia

quite large; the span the entire wing outboard of the Yehudi. They have a chord length of 60-in and span approximately 48-ft.

FIGURE 32 plots up our *VORLAX* computed aerodynamic stability & control database. We ran the code from -5-deg to +12-deg angle-of-attack at Mach 0.3, 0.86 and 1.5. We see that the vehicle has positive weathercock stability ($dCn/d\beta>0$) at all speeds and attitudes; positive effective dihedral ($dCl/d\beta<0$) at all speeds and attitudes, with dihedral effect strongly rising with angle-of-attack; and a rising trend with longitudinal stability ($dCm/d\alpha<0$) at supersonic speeds.

Turning to see FIGURE 33, we can see if we choose a CG position to have ~25% positive static margin at low speeds (justified in FIGURE 34 showing Level I open-loop frequencies at Mach 0.3 per MIL 8785C screening criteria [27]) the aircraft will develop ~55% positive static margin at supersonic cruise (justified in FIGURE 34 (overleaf) showing Level I open-loop frequencies at Mach 1.5 cruise). Since the aircraft does not fly at high angles of attack at supersonic speeds, the elevator deflection to trim is entirely reasonable at cruise ($\delta elev$ <9-deg for α=3-deg at Mach 1.5).

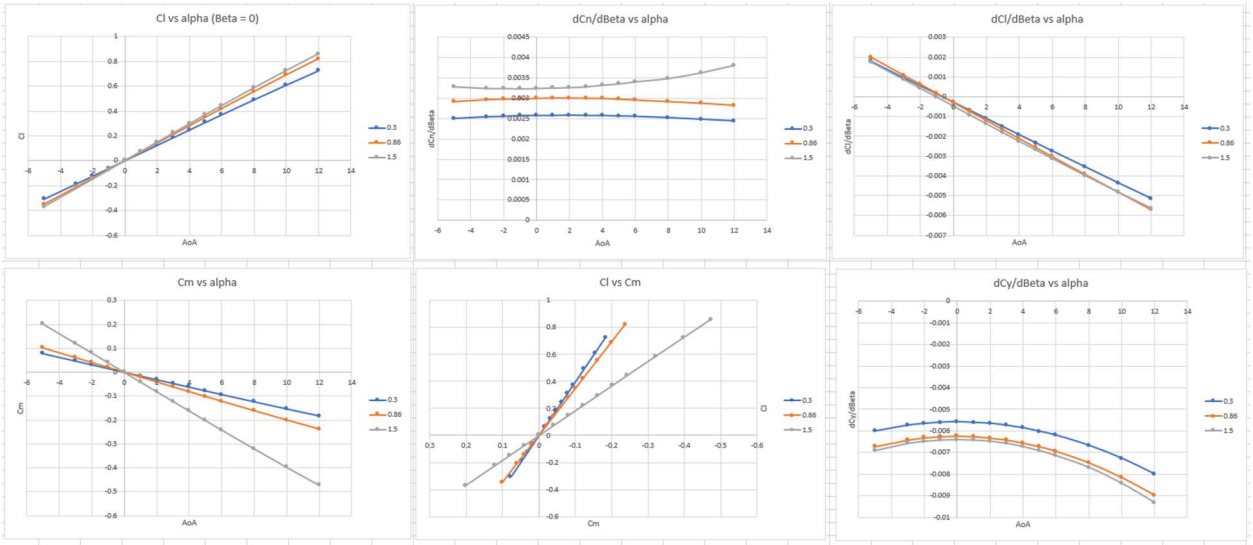

FIGURE 32 - Basic Controls Neutral Stability graphs

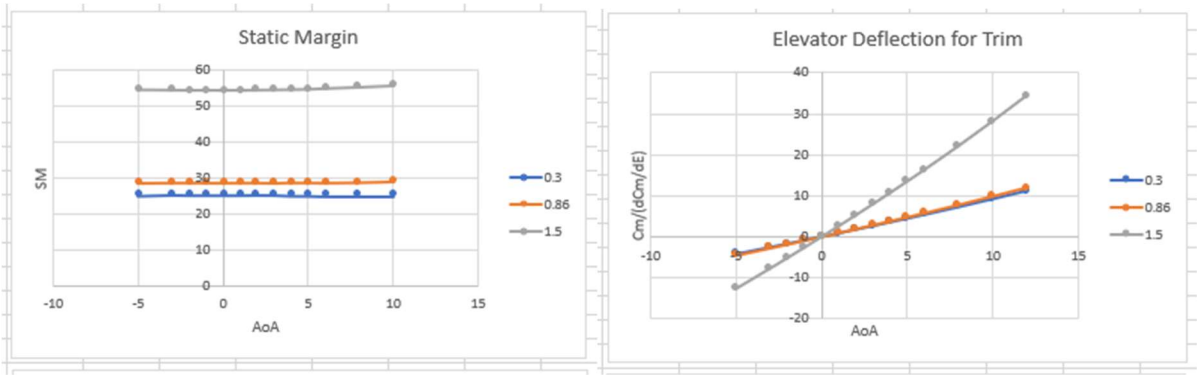

FIGURE 33 – Longitudinal Trim

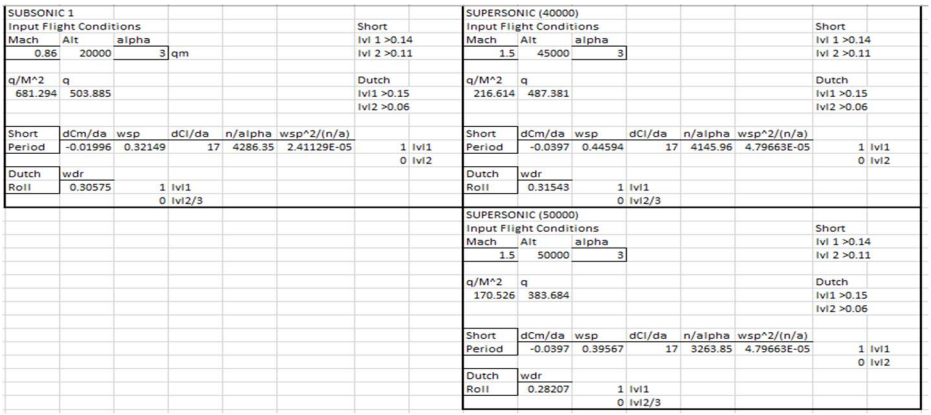

SUBSONIC 1								
Input Flight Conditions							Short	
Mach	Alt	alpha					lvl 1 >0.14	
0.86	20000	3	qm				lvl 2 >0.11	
q/M^2	q						Dutch	
681.294	503.885						lvl1 >0.15	
							lvl2 >0.06	
Short	dCm/da	wsp	dCl/da	n/alpha	wsp^2/(n/a)			
Period	-0.01996	0.32149	17	4286.35	2.41129E-05	1	lvl1	
						0	lvl2	
Dutch	wdr							
Roll	0.30575	1	lvl1					
		0	lvl2/3					

SUPERSONIC (40000)								
Input Flight Conditions							Short	
Mach	Alt	alpha					lvl 1 >0.14	
1.5	45000	3					lvl 2 >0.11	
q/M^2	q						Dutch	
216.614	487.381						lvl1 >0.15	
							lvl2 >0.06	
Short	dCm/da	wsp	dCl/da	n/alpha	wsp^2/(n/a)			
Period	-0.0397	0.44594	17	4145.96	4.79663E-05	1	lvl1	
						0	lvl2	
Dutch	wdr							
Roll	0.31543	1	lvl1					
		0	lvl2/3					

SUPERSONIC (50000)								
Input Flight Conditions							Short	
Mach	Alt	alpha					lvl 1 >0.14	
1.5	50000	3					lvl 2 >0.11	
q/M^2	q						Dutch	
170.526	383.684						lvl1 >0.15	
							lvl2 >0.06	
Short	dCm/da	wsp	dCl/da	n/alpha	wsp^2/(n/a)			
Period	-0.0397	0.39567	17	3263.85	4.79663E-05	1	lvl1	
						0	lvl2	
Dutch	wdr							
Roll	0.28207	1	lvl1					
		0	lvl2/3					

FIGURE 34 – Stability & Control Frequency Analysis

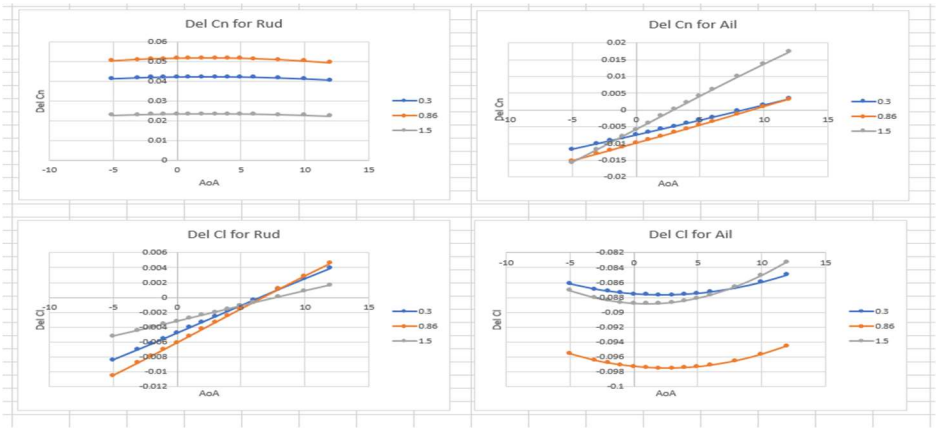

FIGURE 35 – Control Power

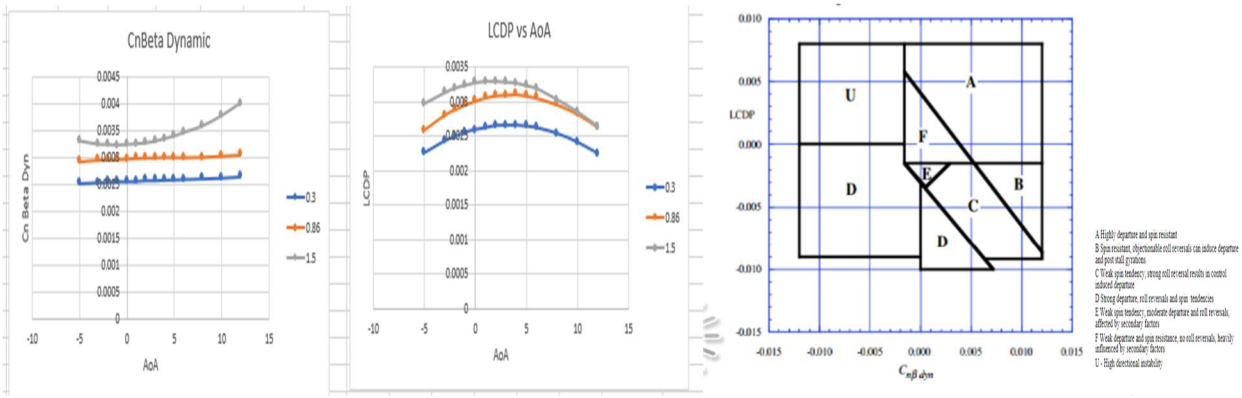

FIGURE 36 – Bihrle-Weissman Chart Build Up

FIGURE 34 also demonstrates that the Dutch Roll frequencies fall within MIL 8785C Level I criteria. [26]

Turning next to FIGURE 35 we see the *VORLAX* database for aileron and rudder effectiveness. We can post-process these results in FIGURE 36 to see that the basic Dutch Roll stability is sufficient to counteract any adverse yaw tendencies of the ailerons based upon the Bihrle-Weissman criteria. Both *Cnβdynamic* and *LCDP* are positive at all speeds and analyzed angles-of-attack placing the aircraft firmly in the "Highly Departure and Spin Resistant" Category "A" on the Weissman Chart.

TABLE 3 – TAKEOFF & LANDING DETAILS

	TAKEOFF
Sref	3,650 ft²
# ENG	4
Static Thrust	52,700 lbf
MTOW	~400,000-lbm
OEW	~210,000-lbm
AR	3.95
W/S @ MTOW	~109 lb/ft²
T/W @ MTOW	~0.53
Ground α	0°
Max Rotation α	16 °
LE Sweep	61.5 °
CLmax	1.2 (free air)
dCL/dα	0.039 /°
CL0	+0.3
ΔCL spoilers	-0.15
CD0	0.0125
ΔCD spoilers	0.0100
ΔCD gear	0.0070
VMCG	135-KEAS
VMCA	125-KEAS
Pitch Rate	4 ° /sec

	LANDING
Sref	3650 ft²
MLW	~285,000-lbm
OEW	~210,000-lbm
AR	3.95
Ground α	0°
Max Rotation α	16 °
LE Sweep	61.5 °
CLmax	1.2
dCL/dα	0.039 /°
CL0	+0.3
ΔCL spoilers	-0.15
CD0	0.0150
ΔCD spoilers	0.0100
ΔCD gear	0.0075
VMCL	129-KEAS
Derotation Time	6-sec

Lateral directional trim control power is sufficient to support an estimated *VMCA* ~ 125 KEAS; *VMCL* ~ 129 KEAS and *VMCG* ~ 135 KEAS.

G. Takeoff and Landing

A hidden problem in aircraft design arises when the aircraft has a low stall speed (from effective take-off flap design) compared to its minimum unstick speed (typically a result when ground angles of attack are limited by tail strike). Highly swept aircraft like the ***Atlantic Shuttle*** also inherently develop vortex lift, which makes for an indistinct stall – and due to high-sweep and modest aspect ratios, have shallow dCL/dα slopes; refer back to FIGURE 28.

Hence, while *CLmax* is not particularly high (*CLmax* estimates for these designs range from 1.0 to 1.2), it occurs at a very high angle of attack. Thus, even with tall landing gear and 14-deg to 16-deg tail strike angles we find *CLmax* in ground-effect limited by tail-strike to be lower than the free-air *CLmax*; see TABLE 3.

Aircraft geometry impacts the effective *CLmax* for takeoff. Recall 14 CFR § 25.107(e) states that *VR* must be the speed that results in the aircraft reaching *V2* at a height of 35-ft above the runway with the critical engine inoperative and a speed not less than the *V1* speed, 105% *VMCA* and 110% *VMU*. With high thrust loadings, even with an inoperative engine, the aircraft will accelerate considerably past the rotation speed as it leaves the runway, we may find ourselves in a situation where the aircraft consistently overshoots its target climb speed, *V2*, based upon a 113% of the free-air stall speed when *VR* is governed by 110% *VMU*.

For the ***Atlantic Shuttle***, the free-air-stall-speed based *V2* speed is impossible to attain given a combination of tail-strike limitations (which elevates *VR*, and the speed gain to 35-ft with a critical engine inoperative). Fowler Flaps needed to be deployed to increase *CL0* simultaneously (and reduce *VMU*), *CLmax* needed to be restricted from +1.2. With the higher wing loading and additional sweep, we had to fully deploy the flaps at takeoff in order to reduce *VMU* to 187-KEAS at MTOW.

We can see with FIGURE 37, the fundamental inaccuracy of Roskam's empirical method; [25] while it reasonably predicts takeoff performance with a short-field schedule at the highest of analyzed weights it does not capture any of the problems arising from *VMU*, *VMCA* and *VMCG* restrictions.

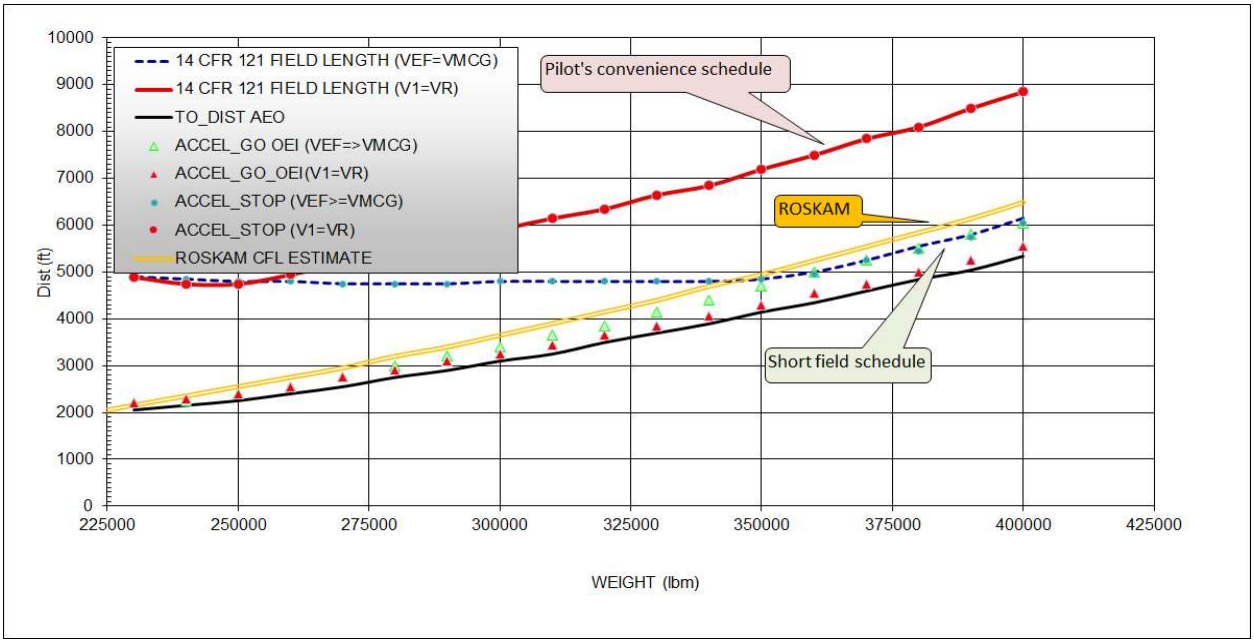

FIGURE 37 – Takeoff Distances – predicted using Roskam as well as Takahashi's time-step-integrating code.

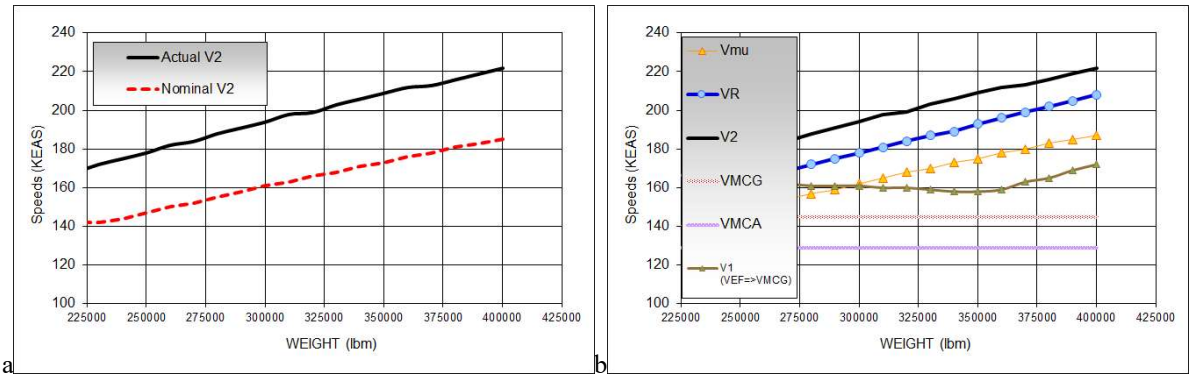

a b

FIGURE 38 – Takeoff Speeds

We can turn next to FIGURE 38 to understand how far off a free-air-stall-speed based estimate of the take-off obstacle clearance speed, *V2* is from the *VMU* restricted reality. We can see from FIGURE 34A that this aircraft diverges further in actual *V2* speeds from the straightforward reading of the 14 CFR § 25.107 rule. Due to *VMU* constraints, the actual *V2* speeds need to be elevated 37 knots above the nominal *V2* at MTOW. Once again, the disconnect in climb speed taints all preliminary design climb performance and noise abatement estimates.

We can see from FIGURE 38b that *VR* tracks 110% *VMU* across a wide range of takeoff weights. At MTOW, *VR* = 110% *VMU* = 208-KEAS. With an aggressive 4-deg/sec pitch rate, even with one-engine inoperative VLOF=220-KEAS to attain *V2*=222-KEAS.

Return to FIGUREs 37 and 38b examine the short-field schedule distance –vs.-weight and *V1* speed –vs.- weight trends. This aircraft is *VMCG* limited over a wide range of weights; beneath 360,000-lbm, *VMCG* limits the decision speed. At MTOW the "Short Field" schedule allows operations from a 6,150-ft runway with *V1*=172-KEAS; once again the "short-field" scheduled takeoff critical field length at heavy weights is actually limited by the 115% all-engines-operating "go" distance

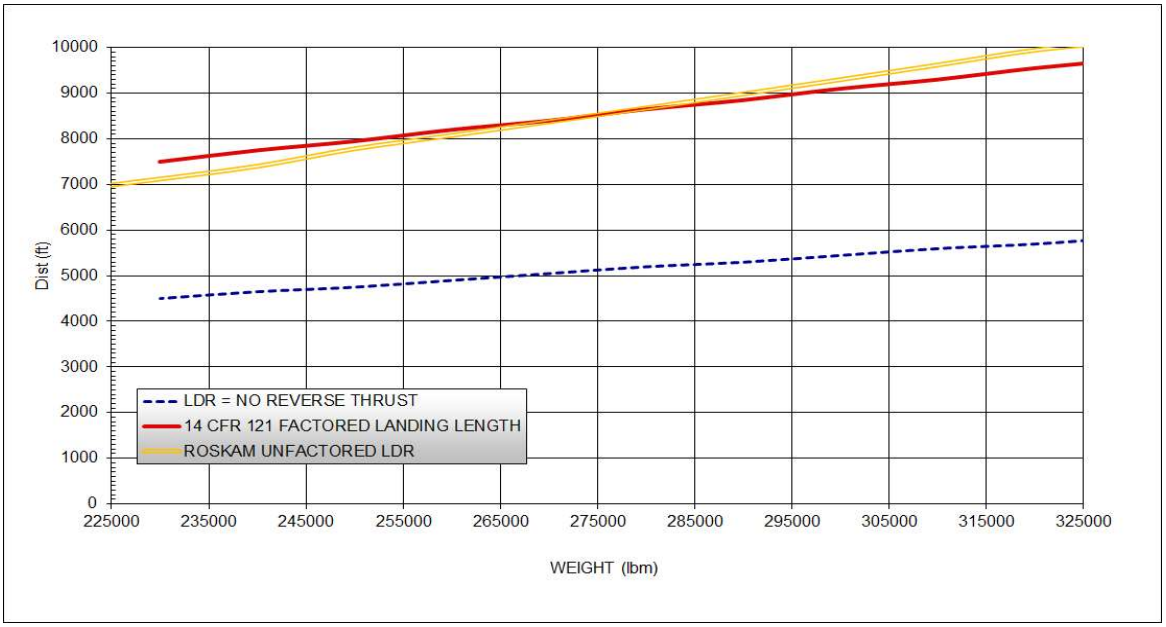

FIGURE 39 – Landing Distances predicted using Roskam as well as Takahashi's time-step integrating code.

Nonetheless, we can see that the dry weather takeoff distances are reasonable with *V1*=VR; at maximum takeoff weight the CFL ~ 8,850-ft. Operationally, this aircraft need not consider a short-field schedule for operations from typical airports.

We also came to realize that Roskam's predicted equations for landing were equally questionable.

The basic time-step integrating landing simulation described in Reference [26] was initially validated against A320 data for the CONF FULL flaps setting in Takahashi, Wood & Bays [32]. Here, we came to realize that Roskam's predicted equations for landing were equally questionable. Our A320 calibration reveals that Roskam's empirical method was based on historical aircraft lacking carbon-fibre brake pads, modern anti-skid systems and current technology tires.

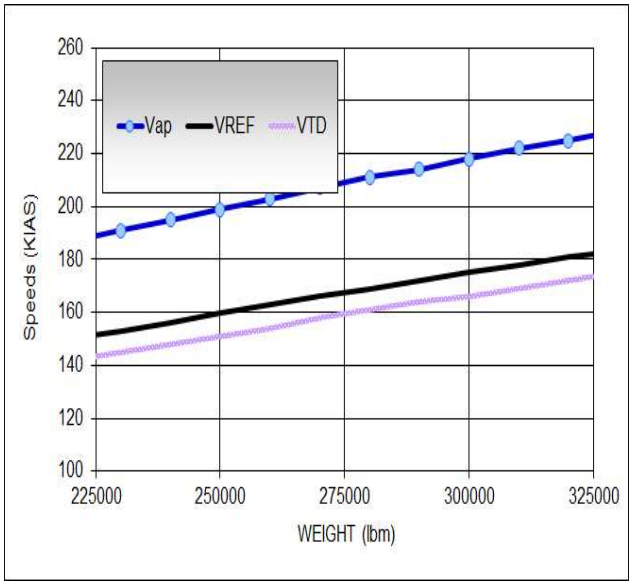

FIGURE 40 – LANDING SPEEDS

Under the revised simulation, we see in FIGURE 35 that despite the long-derotation times arising from a high-angle-of-attack approach, our 14 CFR § 121 factored landing distances ensure that the ***Atlantic Shuttle*** is fully compatible with its intended airports. At a typical touchdown weight around 235,000-lbm the actual landing distance from 50-ft to stop is under 5,000-ft without the use of reverse thrust; the factored landing distances are under 8,000-ft. At our planned maximum landing weight, MLW ~ 285,000-lbm, the factored landing distances are under 9,000-ft. Turning next to FIGURE 36, we can see that *VREF* speeds are always above *VMCA*. With flaps stowed it can fly an initial approach around 190 KEAS (at 235,000-lbm); with flaps deployed it flies *VREF* at ~150 KEAS.

VI. Conclusions

We can see here that the ***Atlantic Shuttle*** meets the customer and mission requirements for speed and operating efficiency. It can fly the North Atlantic in 2 to 3 hours less time than the standard subsonic aircraft even considering routings to avoid over-land sonic booms. We met all stability & control requirements needed to certify for safe flight. Our takeoff and landing distances are compatible with existing airports. We optimized our control surfaces to meet all crosswind regulations and to minimize minimum stall speeds. In conclusion, the aircraft is in compliance with all necessary federal regulations and the fuel burn per seat value of 0.268-lbm/Nm/seat makes it an efficient and affordable alternative to its supersonic predecessors.

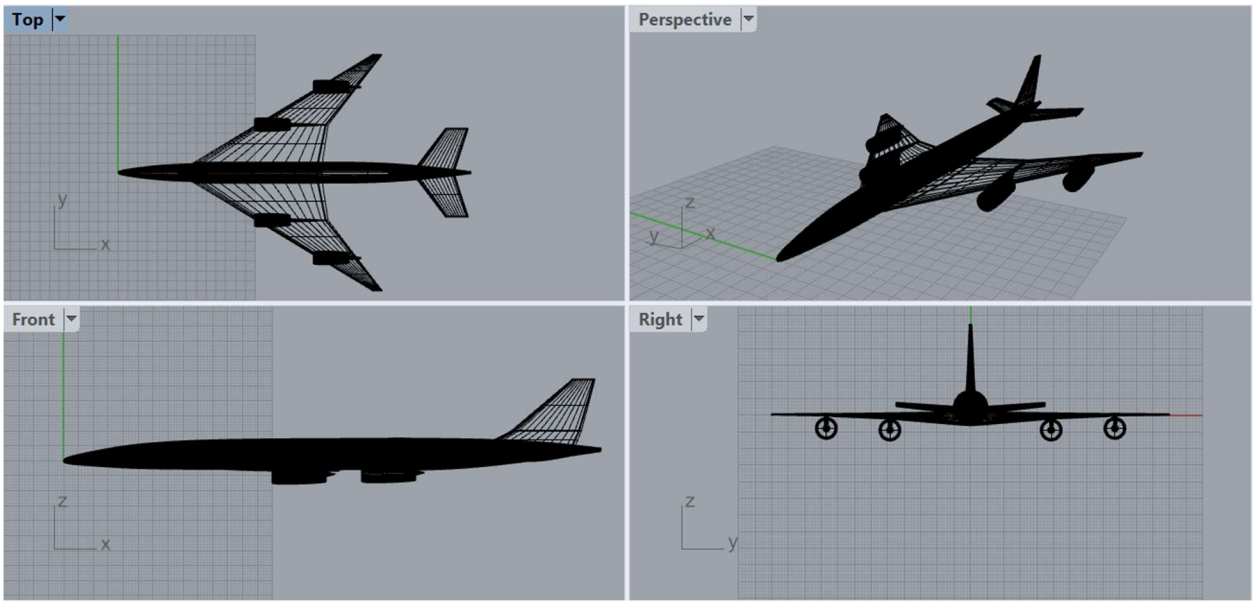

FIGURE 41 – OVERVIEW OF THE *ATLANTIC SHUTTLE*

Acknowledgments

This work began as an unsponsored Senior Capstone Design project performed in partial fulfillment of the degree requirements for obtaining a B.S. in Aerospace Engineering from Arizona State University. Special thanks for Phoenix Integration for supplying Arizona State with *ModelCenter*. Professor Takahashi wishes to thank Wolverine Ventures for supplying *NPSS*.

References

1. https://en.wikipedia.org/wiki/Concorde#cite_note-275
2. https://en.wikipedia.org/wiki/Tupolev_Tu-144
3. https://interestingengineering.com/concorde-the-real-reason-why-the-supersonic-passenger-jet-failed
4. https://en.wikipedia.org/wiki/Transatlantic_flight
5. https://www.schiphol.nl/en/schiphol-as-a-neighbour/page/flight-paths-and-runway-use/
6. http://cohor.fr/web/wp-content/uploads/2013/06/arretes_2003_11_06_CDG_EN.pdf
7. 14 CFR § 25, Airworthiness Standards: Transport Category Airplanes, Code of Federal Regulations. Aeronautics and Space. Revised January 1 2016
8. 14 CFR § 91, General Operating and Flight Rules, Code of Federal Regulations. Aeronautics and Space. Revised January 1 2016.
9. 14 CFR § 121, #, Code of Federal Regulations. Aeronautics and Space. Revised January 1 2016.
10. EASA Certification Specifications CS-25 for Large Aeroplanes (see https://www.easa.europa.eu/certification-specifications/cs-25-large-aeroplanes

11. MIL HDBK 5J
12. Torenbeek, E., *Synthesis of Subsonic Airplane Design*, Delft University Press, Delft, Holland, 1982.
13. Niu, M. C. Y., *Airframe Structural Design, Second Edition,* CONMINLIT Press, Hong Kong, 1997.
14. Takahashi, T., *Aircraft Performance and Sizing, Volume I*, New York, NY: Momentum Press Engineering, 2016
15. Takahashi, T., *Aircraft Performance and Sizing, Volume II*, New York, NY: Momentum Press Engineering, 2016.
16. Boeing 737 Airplane Characteristics for Airport Planning, Boeing D6-58325-6A, 2020. (https://www.boeing.com/commercial/airports/plan_manuals.page)
17. Boeing 747 Airplane Characteristics for Airport Planning, Boeing D6-58326-6E, 2020. (https://www.boeing.com/commercial/airports/plan_manuals.page)
18. NPSS, Numerical Propulsion System Simulation, Software Package, Ver. 2.3.0.1, Ohio Aerospace Institute, Cleveland, OH, 2010.
19. Takahashi, T.T. and Cleary, S.C., "Inlet Diffusor Buoyancy - An Overlooked Term in the Thrust Equation," AIAA 2020-2642, 2020
20. See: https://en.wikipedia.org/wiki/Pratt_%26_Whitney_JT8D
21. ESDU 81024A, "Drag of Axisymmetric Cowls at Zero Incidence For Subsonic Mach Numbers," HIS Engineering Sciences Data Unit, Royal Aeronautical Society, December 1994.
22. Miranda, L. R., Baker, R. D., and Elliott, W. M., "A Generalized Vortex Lattice Method for Subsonic and Supersonic Flow," NASA CR 2875, 1977.
23. Feagin, R. C., and Morrison, W. D., "Delta Method, An Empirical Drag Buildup Technique," NASA Contract Report 151971, 1978.
24. Takahashi, T.T., "Aircraft Concept Design Performance Visualization Using an Energy-Maneuverability Presentation," AIAA 2012-5704, 2012.
25. Lan, CTE and Roskam, J., Airplane Aerodynamics & Performance, DAR Corporation, Lawrence, KS, 2003.
26. Takahashi, T.T., "Development of a Semi-Empirical Takeoff & Landing Method for Supersonic Aircraft," AIAA 2021-0462, 2021.
27. Flying Qualities of Piloted Airplanes, MIL STD-8785C, U.S. Department of Defense, Washington, D.C., Nov. 5, 1980.
28. Equations, Tables and Charts for Compressible Flow, NACA TR-1135, 1953.
29. Mason, W.H., "Analytic Models for Technology Integration in Aircraft Design," AIAA Conference Paper 90-3262, 1990.
30. Day, R.E., *Coupling Dynamics in Aircraft Design*, NASA SP 532, 1997.
31. Roskam, J., Airplane Flight Dynamics & Automatic Controls, Part I, DAR Corporation, Lawrence, KS, 1995.
32. Takahashi, T.T., Wood, D.L. and Bays, L.V., "An Introduction to the Impact of Pilot Techniques Upon "Certified" Field Performance," AIAA 2017-0007, 2017.